




# SARS-CoV-2 Diverges from Other Betacoronaviruses in Only Partially Activating the IRE1 $\alpha$ /XBP1 Endoplasmic Reticulum Stress Pathway in Human Lung-Derived Cells

Long C. Nguyen,<sup>a</sup> David M. Renner,<sup>f,i</sup> Diane Silva,<sup>b</sup> Dongbo Yang,<sup>a</sup> Nicholas A. Parenti,<sup>f,i</sup> Kaeri M. Medina,<sup>f</sup> Vlad Nicolaescu,<sup>c,j</sup> Haley Gula,<sup>c,j</sup> Nir Drayman,<sup>d</sup> Andrea Valdespino,<sup>a</sup> Adil Mohamed,<sup>d</sup> Christopher Dann,<sup>a</sup> Kristin Wannemo,<sup>b</sup> Lydia Robinson-Mailman,<sup>a</sup> Alan Gonzalez,<sup>b</sup> Leticia Stock,<sup>a</sup> Mengrui Cao,<sup>b</sup> Zeyu Qiao,<sup>e</sup> Raymond E. Moellering,<sup>e</sup> Savas Tay,<sup>d</sup> Glenn Randall,<sup>c,j</sup> Michael F. Beers,<sup>g,h</sup> Marsha Rich Rosner,<sup>a</sup> Scott A. Oakes,<sup>b</sup>  Susan R. Weiss<sup>f,i</sup>

<sup>a</sup>Ben May Department for Cancer Research, University of Chicago, Chicago, Illinois, USA

<sup>b</sup>Department of Pathology, University of Chicago, Chicago, Illinois, USA

<sup>c</sup>Department of Microbiology, University of Chicago, Chicago, Illinois, USA

<sup>d</sup>Pritzker School of Molecular Engineering, University of Chicago, Chicago, Illinois, USA

<sup>e</sup>Department of Chemistry, University of Chicago, Chicago, Illinois, USA

<sup>f</sup>Department of Microbiology, University of Pennsylvania, Philadelphia, Pennsylvania, USA

<sup>g</sup>Department of Medicine, University of Pennsylvania, Philadelphia, Pennsylvania, USA

<sup>h</sup>Penn-CHOP Lung Biology Institute, University of Pennsylvania, Philadelphia, Pennsylvania, USA

<sup>i</sup>Penn Center for Research on Coronaviruses and Other Emerging Pathogens, Perelman School of Medicine, University of Pennsylvania, Philadelphia, Pennsylvania, USA

<sup>j</sup>Howard Taylor Ricketts Laboratory, Argonne National Laboratory, Lemont, Illinois, USA

Long C. Nguyen, David M. Renner, and Diane Silva contributed equally.

**ABSTRACT** Severe acute respiratory syndrome coronavirus 2 (SARS-CoV-2) has killed over 6 million individuals worldwide and continues to spread in countries where vaccines are not yet widely available or its citizens are hesitant to become vaccinated. Therefore, it is critical to unravel the molecular mechanisms that allow SARS-CoV-2 and other coronaviruses to infect and overtake the host machinery of human cells. Coronavirus replication triggers endoplasmic reticulum (ER) stress and activation of the unfolded protein response (UPR), a key host cell pathway widely believed to be essential for viral replication. We examined the master UPR sensor IRE1 $\alpha$  kinase/RNase and its downstream transcription factor effector XBP1s, which is processed through an IRE1 $\alpha$ -mediated mRNA splicing event, in human lung-derived cells infected with beta-coronaviruses. We found that human respiratory coronavirus OC43 (HCoV-OC43), Middle East respiratory syndrome coronavirus (MERS-CoV), and murine coronavirus (MHV) all induce ER stress and strongly trigger the kinase and RNase activities of IRE1 $\alpha$  as well as XBP1 splicing. In contrast, SARS-CoV-2 only partially activates IRE1 $\alpha$  through autophosphorylation, but its RNase activity fails to splice XBP1. Moreover, while IRE1 $\alpha$  was dispensable for replication in human cells for all coronaviruses tested, it was required for maximal expression of genes associated with several key cellular functions, including the interferon signaling pathway, during SARS-CoV-2 infection. Our data suggest that SARS-CoV-2 actively inhibits the RNase of autophosphorylated IRE1 $\alpha$ , perhaps as a strategy to eliminate detection by the host immune system.

**IMPORTANCE** SARS-CoV-2 is the third lethal respiratory coronavirus, after MERS-CoV and SARS-CoV, to emerge this century, causing millions of deaths worldwide. Other common coronaviruses such as HCoV-OC43 cause less severe respiratory disease. Thus, it is imperative to understand the similarities and differences among these viruses in how each interacts with host cells. We focused here on the inositol-requiring enzyme 1 $\alpha$  (IRE1 $\alpha$ ) pathway, part of the host unfolded protein response to virus-induced stress.

**Editor** Diane E. Griffin, Johns Hopkins Bloomberg School of Public Health

**Copyright** © 2022 Nguyen et al. This is an open-access article distributed under the terms of the [Creative Commons Attribution 4.0 International license](https://creativecommons.org/licenses/by/4.0/).

Address correspondence to Marsha Rich Rosner, [mrosner@uchicago.edu](mailto:mrosner@uchicago.edu), Scott A. Oakes, [soakes@bsd.uchicago.edu](mailto:soakes@bsd.uchicago.edu), or Susan R. Weiss, [weissr@pennmedicine.upenn.edu](mailto:weissr@pennmedicine.upenn.edu).

The authors declare a conflict of interest. S.R.W. is on the Scientific Advisory Boards of Immunome, Inc and Ocugen, Inc. S.A.O. is a cofounder and consultant at OptiKira, L.L.C. (Cleveland, OH) R.E.M. is a founder and consultant at ReAx Biotechnologies (Chicago, IL) and Anastasis Biotech (London, UK).

This article is a direct contribution from Susan R. Weiss, a Fellow of the American Academy of Microbiology, who arranged for and secured reviews by Shinji Makino, The University of Texas Medical Branch, and Luis Enjuanes, Centro Nacional de Biotecnología, CNB-CSIC.

**Received** 30 August 2022

**Accepted** 30 August 2022

We found that while MERS-CoV and HCoV-OC43 fully activate the IRE1 $\alpha$  kinase and RNase activities, SARS-CoV-2 only partially activates IRE1 $\alpha$ , promoting its kinase activity but not RNase activity. Based on IRE1 $\alpha$ -dependent gene expression changes during infection, we propose that SARS-CoV-2 prevents IRE1 $\alpha$  RNase activation as a strategy to limit detection by the host immune system.

**KEYWORDS** IRE1 $\alpha$  pathway, MERS-CoV, OC43, SARS-CoV-2, coronavirus, unfolded protein response

Severe acute respiratory syndrome coronavirus 2 (SARS-CoV-2) emerged in China in late 2019. It was the third lethal zoonotic coronavirus to emerge into humans, after SARS-CoV (2002) and Middle East respiratory syndrome coronavirus (MERS-CoV) (2012), each of which has been associated with acute lung injury and hypoxemic respiratory failure. While coronaviruses are divided into four genera (alpha, beta, gamma, and delta) (1, 2), all three of the lethal human coronaviruses are betacoronaviruses, albeit from different subgenera (Fig. 1). SARS-CoV and SARS-CoV-2 are sarbecoviruses, while MERS-CoV is a merbecovirus. Other human CoVs, including HCoV-OC43 (OC43) and HCoV-HKU1 (HKU-1), are embecoviruses, as is the model murine coronavirus mouse hepatitis virus (MHV). All CoVs have similar genome structures and replication cycles, and the human CoVs as well as some MHV strains exhibit tropism for the epithelia of the respiratory tract, the portal of entry. They replicate their RNAs and produce subgenomic mRNAs by conserved mechanisms and encode homologous structural as well as replicase proteins. Despite the similarities among all coronaviruses, each subgenus expresses distinct accessory proteins that may confer differences in host-virus interactions. Indeed, we have previously found that SARS-CoV-2, MERS-CoV, and MHV all induce somewhat different levels of activation and/or antagonism of interferon (IFN) signaling and other double-stranded RNA (dsRNA) induced antiviral innate responses (3–11).

One key pathway involved in the virus-induced host response is the endoplasmic reticulum (ER) stress response that regulates protein homeostasis (referred to as proteostasis) in this organelle. One-third of all eukaryotic proteins, including most that are inserted into membranes or secreted, are synthesized through co-translational translocation into the ER lumen. Likewise, viral membrane-associated proteins are translated and processed in association with the ER (12, 13). Once in the ER, these polypeptides undergo stringent quality control monitoring to ensure that they are properly processed and folded. If the capacity to fold proteins is unable to keep up with demand, misfolded proteins will accumulate in the ER lumen—a condition referred to as “ER stress.” The presence of misfolded proteins in the ER is sensed by three transmembrane sentinel proteins—activating transcription factor 6 (ATF6), PKR-like ER kinase (PERK), and inositol-requiring enzyme (IRE)1 $\alpha$ —which trigger an intracellular signaling pathway called the unfolded protein response (UPR). In an effort to restore proteostasis, activation of these sensors induces transcription factors that turn on genes encoding chaperones, oxidoreductases, and ER-associated decay (ERAD) components (14). The UPR also inhibits cap-dependent translation, thus decreasing the load on the ER and giving it extra time to fold proteins already in production (15, 16). If successful, these adaptive UPR programs restore ER homeostasis.

The most ancient UPR pathway is controlled by IRE1 $\alpha$ —an ER transmembrane bifunctional kinase/endoribonuclease (RNase) that employs autophosphorylation to control its catalytic RNase function (17, 18). In response to ER stress, IRE1 $\alpha$  undergoes autophosphorylation and dimerization to allosterically activate its RNase domain to excise a 26-nucleotide (nt) nonconventional intron in *XBP1* mRNA; religation of spliced *XBP1* shifts the open reading frame, and its translation produces the homeostatic transcription factor XBP1s (*s* = spliced) (19, 20). Once synthesized, XBP1s upregulates genes that expand the ER and its protein folding machinery (21). IRE1 $\alpha$  can additionally lead to apoptosis and inflammation via JUN N-terminal kinase (JNK) and p38 mitogen-activated protein

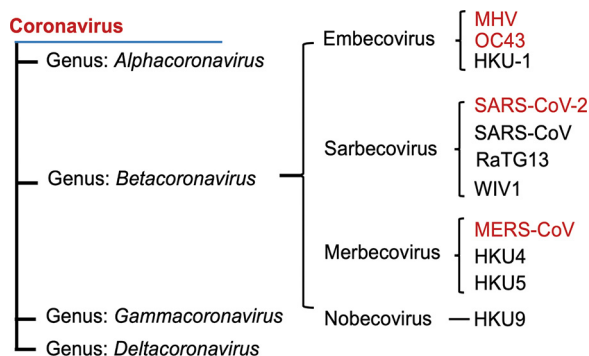


**FIG 1** Coronavirus family. Phylogenetic tree of betacoronaviruses and their subgenera. Viruses examined in this study are shown in red font.

kinase (MAPK) signaling (22). Prolonged ER stress can induce regulated IRE1-dependent decay (RIDD), promoting the cleavage of additional targets beyond XBP1 mRNA, such as secretory protein and ER-localized mRNAs (23). In the short term, RIDD may promote adaptation through further reducing translation and the protein burden on the ER. However, prolonged RIDD leads to the depletion of vital ER resident enzymes and structural components to exacerbate ER stress and hasten cell death (17, 24).

There is a large body of evidence that viral replication in mammalian cells can trigger ER stress and UPR activation in infected cells (25), and numerous studies report that the UPR is activated upon infection of host cells by coronavirus family members (12, 13, 26–31). Coronaviruses induce stress in the ER in several ways. First, conserved replicase-encoded, nonstructural proteins nsp3, nsp4, and nsp6 are embedded into the ER membrane and, along with unknown host factors, promote membrane curvature to form double membrane vesicles (DMVs), the site of viral replication/transcription centers (RTC) (32). In addition to remodeling the ER, coronaviruses further condition infected cells by shifting translation away from host mRNAs and instead to viral mRNAs. Translation of viral mRNAs causes the ER to be flooded with heavily glycosylated viral structural proteins (e.g., spike [S], membrane [M], and envelope [E]), challenging the organelle's folding capacity and overall integrity. Indeed, overexpression of coronavirus spike proteins (33) as well as several sarbecovirus accessory proteins (28, 34), has been reported to induce ER stress, although overexpression itself may cause stress irrespective of the proteins. Finally, cell membranes are depleted as enveloped virus particles are assembled into new virions in the ER-Golgi intermediate compartment before budding from the infected cell (1). Thus, coronaviruses as well as other enveloped viruses promote a massive ER expansion and modification necessary to replicate their genomes, transcribe mRNAs, and finally, to process and package their protein products into viral particles.

We have compared the activation status and requirement of the IRE1 $\alpha$ /XBP1 arm of the UPR in well-characterized human lung epithelial cell lines and in induced pluripotent stem cell (iPSC)-derived type II alveolar (iAT2) cells, following infection with four betacoronaviruses representing three distinct subgenera. We find that infection with MERS-CoV, OC43, and MHV leads to phosphorylation of IRE1 $\alpha$  and the consequent production of spliced XBP1 (XBP1s) transcription factor. Surprisingly, while we observed phosphorylation of IRE1 $\alpha$  in SARS-CoV-2 infected cells, there was a notable absence of XBP1s, suggesting that SARS-CoV-2 inhibits downstream signaling of the IRE1 $\alpha$ /XBP1 arm of the UPR. In addition, we report reduced SARS-CoV-2-induced interferon signaling gene expression in the absence of IRE1 $\alpha$ .

## RESULTS

**Induction of IRE1 $\alpha$  phosphorylation following coronavirus infection.** To determine whether betacoronaviruses activate IRE1 $\alpha$ , we first examined the level of phosphorylated IRE1 $\alpha$  after viral infection of the A549 human lung carcinoma cell line. We

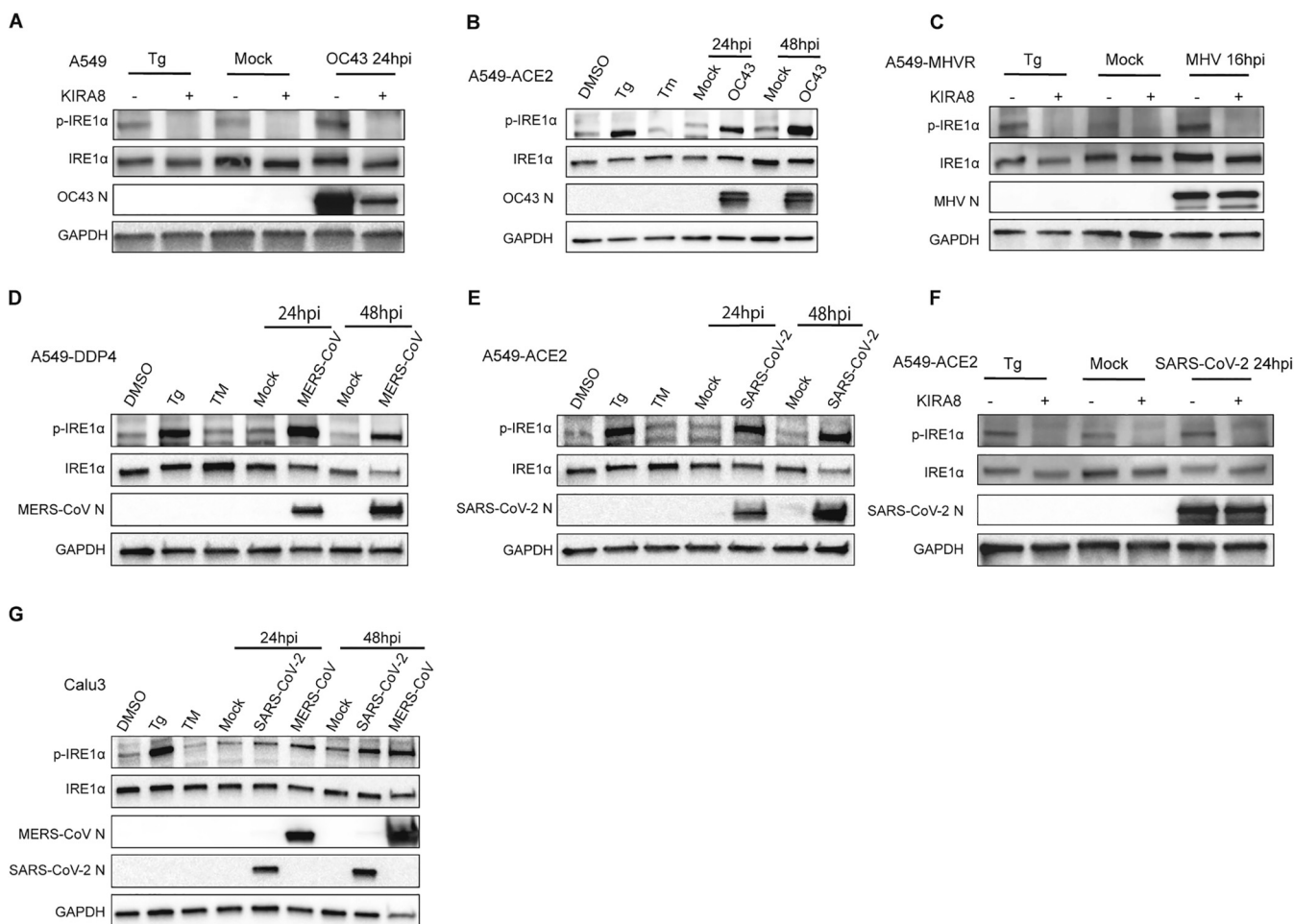


**FIG 2** Induction of IRE1 $\alpha$  phosphorylation following coronavirus infection. A549 cells expressing the indicated viral receptors were mock infected or infected. Protein was harvested at 16, 24, or 48 hpi and analyzed by immunoblotting with antibodies, as indicated. (A, C, and F) Cells infected with OC43 (A), MHV (C), or SARS-CoV-2 (F) at an MOI of 5 were pretreated 2 h prior to infection with 1  $\mu$ M KIRA8. (B, D, and E) Cells were infected with OC43 at an MOI of 1 (B), MERS-CoV at an MOI of 5 (D), or SARS-CoV-2 at an MOI of 5 (E) or treated with DMSO, thapsigargin (Tg; 1  $\mu$ M) for 1 h or tunicamycin (TM, 1  $\mu$ g/mL) for 8 h. (G) Calu-3 cells were mock infected or infected with MERS-CoV or SARS-CoV-2 (MOI, 5). Data shown are from one representative of at least two independent experiments.

used A549 cells stably expressing the following receptors to facilitate optimal entry for each of the viruses: carcinoembryonic antigen cell adhesion molecule (CEACAM) 1a or MHVR (MHV), dipeptidyl peptidase DPP4 (MERS-CoV) or angiotensin-converting enzyme 2 (ACE2) (SARS-CoV-2). HCoV-OC43 can infect parental A549 or cells expressing ACE2 (3). Consistent with previous reports that embeco subgenus coronaviruses MHV (26, 35) and OC43 (30) induce ER stress, we observed a significant increase in phospho-IRE1 $\alpha$  (p-IRE1 $\alpha$ ) during infection by either OC43 (24 or 48 h postinfection [hpi]) or MHV (24 hpi) (Fig. 2A to C). To confirm the specificity of the p-IRE1 $\alpha$  band, we pretreated cells prior to infection with KIRA8, a highly selective kinase inhibitor of IRE1 $\alpha$  known to inhibit both autophosphorylation and, consequently, RNase activity. As expected, KIRA8 significantly inhibited the induction of p-IRE1 $\alpha$  by OC43 and MHV (Fig. 2A and C). Thapsigargin (Tg) and tunicamycin (TM), both inducers of ER stress, were used as further controls (Fig. 2B and D, and E). Robust induction of p-IRE1 $\alpha$  was observed with 1 h of Tg (1  $\mu$ M) treatment, while no activation of p-IRE1 $\alpha$  was observed after 8 h of treatment with TM (1  $\mu$ g/mL), consistent with the negative feedback regulation observed with extended TM treatment (36). We also observed robust phosphorylation of IRE1 $\alpha$  in A549-DDP4 cells and A549-ACE2 cells infected by MERS-CoV and SARS-CoV-2, respectively, at 24 and 48 hpi (Fig. 2D to F and Fig. S1A and B in the supplemental material). As with OC43 and MHV, IRE1 $\alpha$  phosphorylation during SARS-CoV-2 infection was inhibited by KIRA8

(Fig. 2F). Interestingly, we observed a decrease in OC43 (Fig. 2A) and SARS-CoV-2 (Fig. 2F) nucleocapsid expression in KIRA8-treated cells. However, this may be the result of off-target effects from the compound rather than solely from IRE1 $\alpha$  inhibition, given our findings described below using IRE1 $\alpha$  knockout (KO) cells. These results are not limited to a single cell type, as we observed similar induction of p-IRE1 $\alpha$  in Calu-3 cells, another lung epithelial-derived cells line, which can be productively infected with both MERS-CoV or SARS-CoV-2 (Fig. 2G). These results demonstrate that MERS-CoV, SARS-CoV-2, HCoV-OC43, and MHV activate the host IRE1 $\alpha$  kinase after infection.

#### **MHV, OC43, and MERS-CoV but not SARS-CoV-2 induce splicing of XBP1 mRNA.**

We next examined the effect of coronavirus infection on the RNase activity of IRE1 $\alpha$  as assessed by XBP1 splicing. Using specific primers to quantify spliced XBP1 mRNA (XBP1s), we observed a marked increase in the percentage of spliced XBP1 mRNA (%XBP1s) as well as an increase in the relative amount of spliced XBP1 mRNA (XBP1s) compared to the mock control after infection by OC43, MERS-CoV, or MHV in receptor-expressing A549 cells (Fig. 3A and B and Fig. S2A and B). This induction of XBP1s by OC43 and by MERS-CoV infection was confirmed by assessing XBP1 splicing by agarose gel electrophoresis (Fig. 3E and F). DNAJB9, a canonical target of XBP1s, was also markedly upregulated with OC43, MERS-CoV, and MHV infection at both 24 and 48 hpi (Fig. 3A and B and Fig. S2B). This induction of IRE1 $\alpha$  RNase activity is coincident with the observed autophosphorylation of p-IRE1 $\alpha$  upon OC43, MHV, or MERS-CoV infection.

Surprisingly, despite the observed IRE1 $\alpha$  autophosphorylation following SARS-CoV-2 infection, there was no significant upregulation of XBP1s mRNA in A549-ACE2 cells up to 52 hpi (Fig. 3C and G). Similarly, DNAJB9 expression levels were unchanged at all time points observed with SARS-CoV-2 (Fig. 3C). To confirm that this effect is not limited to A549 cells, we measured XBP1 mRNA splicing in MERS-CoV- and SARS-CoV-2-infected Calu-3 cells. Again, infection with MERS-CoV, but not SARS-CoV-2, significantly induced XBP1s and its downstream effector DNAJB9 (Fig. 3D and H). In agreement with these results, OC43, but not SARS-CoV-2, infection induced XBP1s protein levels (Fig. 3I and J).

**Upon infection, MHV, OC43, and MERS-CoV induce IRE1 $\alpha$  and related genes to a greater extent than SARS-CoV-2.** To determine how different coronaviruses impact the UPR at the transcriptional level, we performed RNA-sequencing of A549-DPP4 cells infected with MERS-CoV for 24 and 36 h. We compared the results to published RNA sequencing (RNA-seq) data sets (35, 37) of MHV infection of murine bone marrow-derived macrophages (BMDM) or SARS-CoV-2 infection of A549-ACE2, normal human bronchial epithelial (NHBE) cells, and Calu-3 cell lines. In agreement with our IRE1 $\alpha$  activation results, Ingenuity Pathway Analysis (IPA) predicted activation of the UPR and ER stress pathways by MERS-CoV and MHV (Fig. 4A). In contrast, SARS-CoV-2 consistently showed little to no activation of the UPR and ER stress pathway across different multiplicity of infection (MOI) conditions and cell lines.

To confirm the results of the gel electrophoresis splicing assays for XBP1 mRNA that distinguished SARS-CoV-2 infection from that of the other betacoronaviruses (Fig. 3), we further utilized the RNA-seq results to quantitatively measure XBP1 mRNA splicing by these coronaviruses. Through RNA-seq, we visualized both the unspliced and spliced XBP1 mRNA reads based on whether they contain the 26-nucleotide nonconventional intron that is removed as a result of RNase activity of IRE1 $\alpha$  as previously described (38) (Fig. 4B and C). MERS-CoV infection resulted in significant XBP1 mRNA splicing, in contrast to no difference detected in SARS-CoV-2-infected versus mock-infected cells (Fig. 4B and C). We further quantified total XBP1 spliced versus unspliced reads, which consistently showed a substantial increase in the percent expression of the XBP1s reads when normalized to total XBP1 reads for MERS-CoV at both 24 and 36 hpi but not for SARS-CoV-2-infected cells (Fig. 4D and E). This was consistent with significant upregulation of DNAJB9 and total XBP1 during infection with MERS-CoV but not SARS-CoV-2 (Fig. 4F to I).

**MERS-CoV but not SARS-CoV-2 induces XBP1 splicing during infection of biologically relevant iPSC-derived alveolar type II cells.** To confirm our results in a more physiologically relevant cell, we infected iPSC-derived type II alveolar (iAT2) cells.

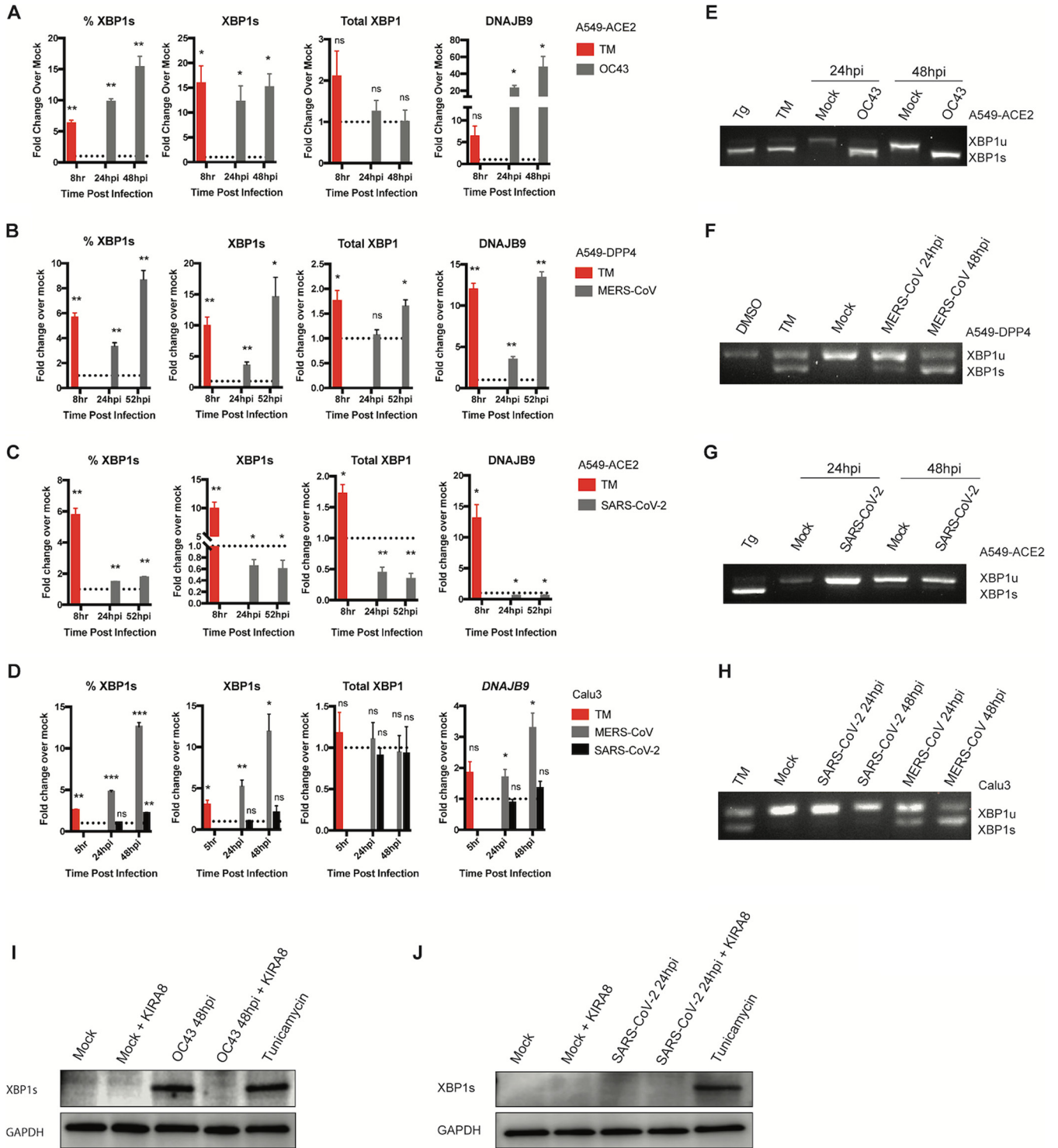


**FIG 3** IRE1 $\alpha$ -mediated XBP1 splicing occurs following infection with OC43 or MERS-CoV, but not SARS-CoV-2. (A to C, E to G) A549 cells were mock infected or infected (in triplicate) with OC43 at an MOI of 1 (A, E), MERS-CoV at an MOI of 5 (B, F), or SARS-CoV-2 at an MOI of 5 (C, G) or treated with TM (1  $\mu$ g/mL) for 8 h, and total RNA was harvested at the indicated time points. (A to C) Relative %XBP1s, XBP1s, total XBP1, and DNAJB9 mRNA expression were quantified by RT-qPCR.  $C_T$  values were normalized to 18S rRNA and expressed as the fold change over the mock control displayed as  $2^{-\Delta(\Delta C_T)}$ . Technical replicates were averaged, and the means for each replicate were displayed  $\pm$  the standard deviation (SD; error bars). (D) Calu-3 cells were mock infected or infected with MERS-CoV or SARS-CoV-2 (MOI, 5) and total RNA was harvested at the indicated time points. Relative %XBP1s, XBP1s and total XBP1 and DNAJB9 mRNA expression were quantified by RT-qPCR, calculated, and displayed as described above. Values are means  $\pm$  SD (error bars). Statistical significance was determined using two-tailed, paired Student's *t* test. Displayed significance (infected relative to mock) is determined by the *P* value; \*, *P* < 0.05; \*\*, *P* < 0.01; \*\*\*, *P* < 0.001; \*\*\*\*, *P* < 0.0001; ns, not significant. (E to H) RNA was harvested from A549 cells mock infected or infected with OC43 at an MOI of 1 (E), MERS-CoV at an MOI of 5 (F), SARS-CoV-2 at an MOI of 5 (G), or Calu-3 cells infected with MERS-CoV and SARS-CoV-2 at an

(Continued on next page)

We employed the SPC2 line, which expresses tdTomato from the surfactant protein-C (SFTPC) locus as an AT2 marker, which we have previously used to characterize innate immune responses to SARS-CoV-2 infection (3). Type II alveolar cells are a major target during both MERS-CoV and SARS-CoV-2 infection in humans, and their destruction may be a contributing factor to lung pathogenesis in severe cases (39, 40).

Both MERS-CoV and SARS-CoV-2 replicate in these cells and release infectious virus as quantified by plaque assay (Fig. 5A). Notably, MERS-CoV replicated to higher titers than SARS-CoV-2 in these lung-derived cells. This complements our previous findings that SARS-CoV-2 replicates more efficiently than MERS-CoV in upper respiratory-derived primary nasal cells (3) and may suggest that MERS-CoV is better adapted to replicate within the lower respiratory tract while SARS-CoV-2 replicates more efficiently in the upper airway. Despite this difference in replication, both viruses were observed to induce p-IRE1 $\alpha$  over the course of infection (Fig. 5B). In agreement with our results in A549 and Calu-3 cells, SARS-CoV-2 failed to induce XBP1 splicing in iAT2 cells, as measured by reverse transcription quantitative PCR (RT-qPCR) (Fig. 5C). In contrast, MERS-CoV induced XBP1 splicing, albeit to a lower extent than in immortalized cell lines. Lastly, we visualized XBP1 splicing using reverse transcriptase PCR (RT-PCR) and agarose gel electrophoresis (Fig. 5D). Again, our data indicate that SARS-CoV-2 fails to induce XBP1 splicing at either 24 or 48 hpi in iAT2 cells, despite inducing p-IRE1 $\alpha$ . MERS-CoV, however, induced increasing XBP1 splicing over the course of infection, matching the results in A549 and Calu-3 cells (Fig. 2 and 3). Overall, these results indicate that both SARS-CoV-2 and MERS-CoV induce ER stress as evidenced by IRE1 $\alpha$  phosphorylation during infection of primary iAT2 cells, but only MERS-CoV induces the downstream effects of active IRE1 $\alpha$  RNase.

**SARS-CoV-2 inhibits XBP1 splicing.** We then tested whether SARS-CoV-2 actively inhibits splicing of XBP1 induced by the N-linked glycosylation inhibitor tunicamycin (TM), a common agent used to chemically induce ER stress. To do so, A549-ACE2 cells were either mock infected or infected with SARS-CoV-2 or OC43 for 24 h and then treated with TM for 6 h prior to analysis. Interestingly, while SARS-CoV-2 infection did not completely prevent XBP1 splicing induced by TM, it led to significantly lower XBP1 splicing levels compared with mock infected cells (Fig. 6A). Furthermore, this inhibition is not due to a reduction in phosphorylation of IRE1 (Fig. S3A). In contrast, OC43 increased XBP1 splicing at all tested concentrations of TM (Fig. 6B). This suggests that SARS-CoV-2 actively inhibits activation of the IRE1 $\alpha$  RNase.

**Betacoronaviruses do not require IRE1 $\alpha$  for replication.** Given the presumed importance of IRE1 $\alpha$ /XBP1s to expand the ER and maintain protein folding during viral replication, and the interesting differences we observed between SARS-CoV-2 and the other betacoronaviruses, we next explored the consequences of its inhibition on the replication of each virus. To determine whether IRE1 $\alpha$  activity is required for replication and propagation of MHV, OC43, MERS-CoV, or SARS-CoV-2, we utilized CRISPR/Cas9 gene editing to knock out IRE1 $\alpha$  in A549 cell lines expressing receptors for each coronavirus (Fig. S3B to G). Surprisingly, we did not observe any significant differences in the capability of all tested coronaviruses to replicate in cells lacking IRE1 $\alpha$  (Fig. 6C to F). These results suggest IRE1 $\alpha$  is neither essential nor inhibitory for coronavirus replication in these cells. Since SARS-CoV-2 does not lead to IRE1 $\alpha$ -mediated XBP1 splicing, we also tested replication of SARS-CoV-2 and OC43 in XBP1 KO cells (Fig. 6C and D and Fig. S3H). Consistently, there was no detectable effect of XBP1 KO on SARS-CoV-2 or OC43 replication in A549-ACE2 cells. Together, these results demonstrate that none of

### FIG 3 Legend (Continued)

MOI of 5 (H) or treated with tunicamycin (TM; 1  $\mu$ g/mL) for 8 h, or thapsigargin (Tg; 1  $\mu$ M) for 1 h or DMSO. RT-PCR was performed using primers crossing the XBP1 splicing site. The product was resolved on an agarose gel to visualize XBP1 splicing. (I to J) Lysates from A549-ACE2 cells mock infected, treated with TM (500 ng/mL) for 6 h, or infected with OC43 (MOI, 4) or SARS-CoV-2 (MOI, 3) with or without KIRA8 (1  $\mu$ M) treatment were harvested at the indicated time points as in Fig. 2A, C and F and immunoblotted with antibody against XBP1s protein. Data shown are from one representative experiment from at least three independent experiments.

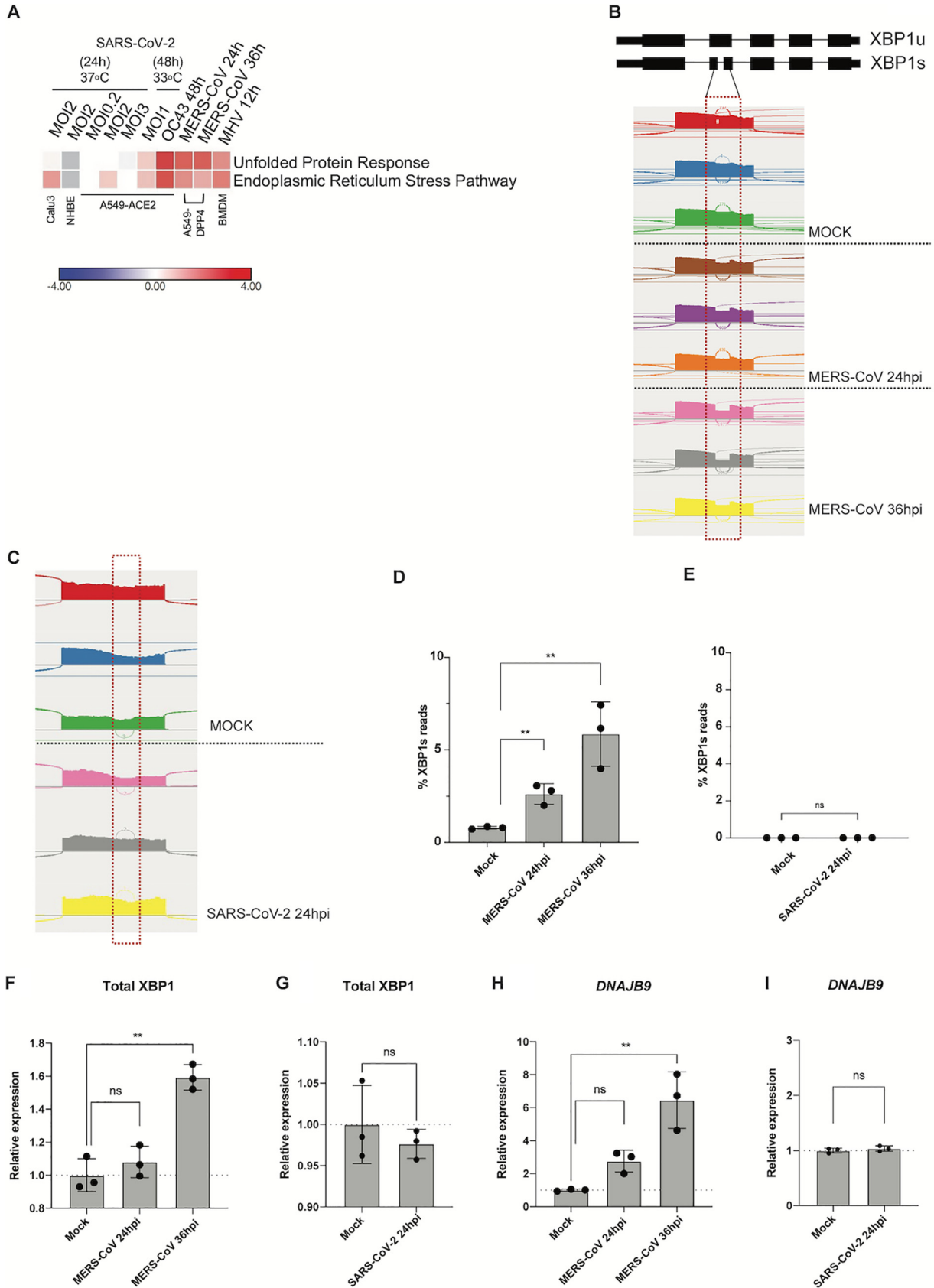


**FIG 4** Unlike other coronaviruses, SARS-CoV-2 infection does not lead to robust UPR activation. (A) Heatmap of predicted pathway status based on Ingenuity Pathway Analysis (IPA) of activation Z-scores for each pathway from RNA-sequencing data from the indicated cells (Continued on next page)



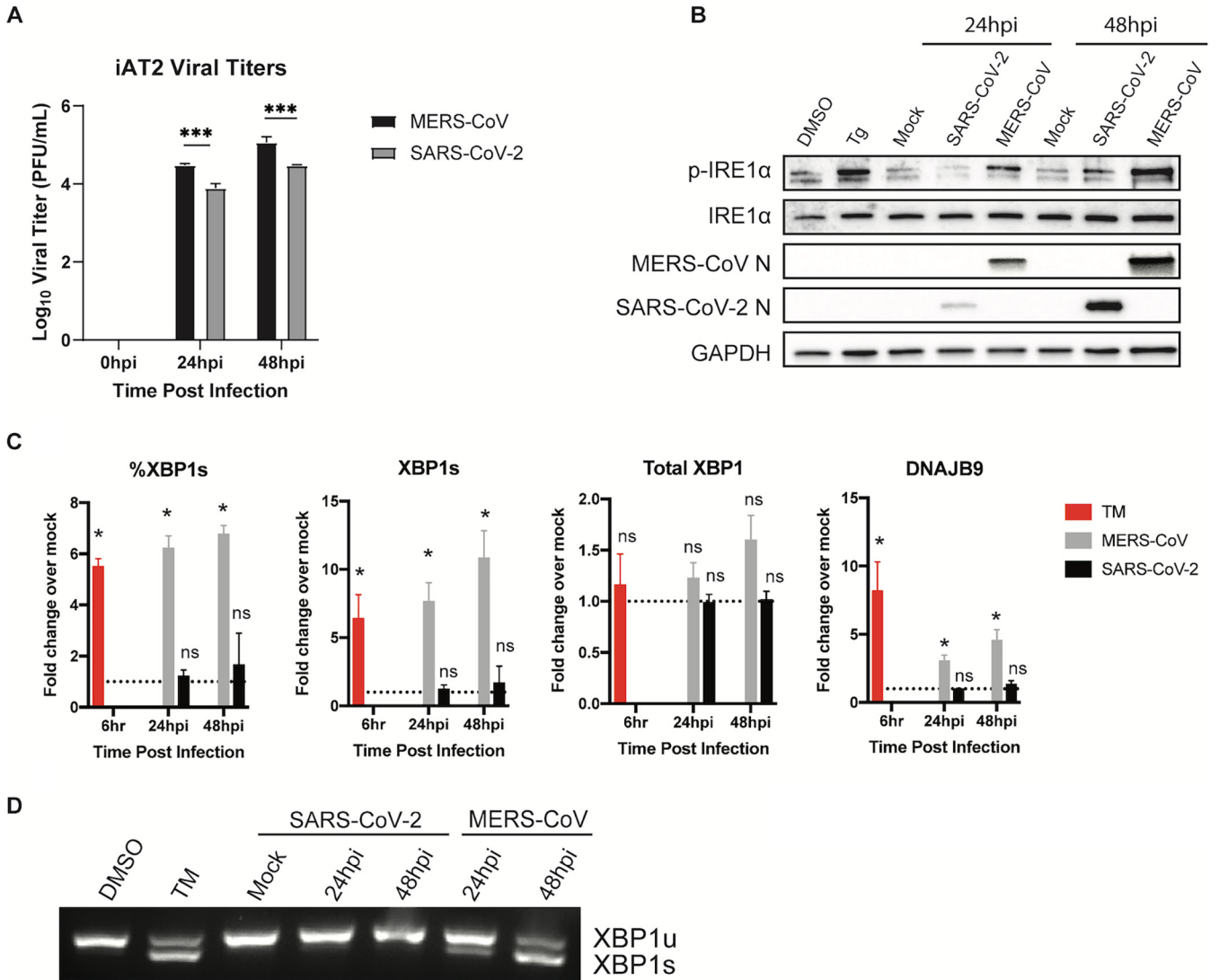


**FIG 5** SARS-CoV-2 and MERS-CoV induce IRE1 $\alpha$  phosphorylation in iAT2 cells but diverge in induction of XBP1 splicing. iPSC-derived AT2 cells (iAT2 cells) were mock infected or infected (in triplicate) with MERS-CoV or SARS-CoV-2 at an MOI of 5. (A) At the indicated time points, supernatants were collected, and infectious virus was quantified by plaque assay. Values are means  $\pm$  SD (error bars). Statistical significance was determined by two-way ANOVA (\*,  $P < 0.05$ ; ns, not significant). (B) Total protein was harvested at the indicated time points and analyzed by immunoblotting using the indicated antibodies. Thapsigargin treatment for 1 h (Tg; 1  $\mu$ M) was used as a positive control for IRE1 $\alpha$  activation, while DMSO served as a vehicle control. (C) Total RNA was harvested at the indicated time points and relative %XBP1s, XBP1s, and total XBP1 mRNA expression were quantified by RT-qPCR, calculated, and displayed as described above. Values are means  $\pm$  SD (error bars). Statistical significance (infected compared to mock) was determined using two-tailed, paired Student's  $t$  test. Displayed significance is determined by the  $P$  value; \*,  $P < 0.05$ ; \*\*,  $P < 0.01$ ; \*\*\*,  $P < 0.001$ ; \*\*\*\*,  $P < 0.0001$ ; ns, not significant. (D) RT-PCR was performed using extracted RNA and primers crossing the XBP1 splicing site. The product was run out on an agarose gel to visualize XBP1 splicing. Tunicamycin treatment (1  $\mu$ g/mL for 6 h) was used as a positive control for RT-(q)PCR, while DMSO treatment served as a vehicle control. Data shown are from one representative experiment from at least two independent experiments.

the coronaviruses tested require the activation IRE1 $\alpha$ /XBP1 pathway for optimal replication.

**Loss of IRE1 $\alpha$  expression causes robust alterations in gene expression, including reduced interferon signaling, following SARS-CoV-2 infection.** To gain insight

**FIG 4** Legend (Continued)

infected with OC43 (MOI, 1), MERS-CoV (MOI, 1), MHV (MOI, 1), and SARS-CoV-2 under the specified conditions. Red, pathway predicted to be activated; blue, pathway predicted to be inhibited; white, pathway predicted to be unchanged; gray, no prediction due to lack of significance. (B and C) Quantification of XBP1 splicing by analyzing RNA-seq data from A549-DPP4 and A549-ACE2 cells mock infected or infected with MERS-CoV or SARS-CoV-2, respectively, under the indicated conditions. Reads representing spliced or unspliced XBP1 mRNA were identified based on the presence or absence of the 26-nucleotide intron and quantified. (D to I) Percentage of XBP1 spliced reads or relative expression of total XBP1 and DNAJB9 mRNA from the RNA-seq samples. Values are means  $\pm$  SD (error bars). Statistical significance was determined by unpaired  $t$  tests (\*,  $P < 0.05$ ; \*\*,  $P < 0.01$ ; ns, not significant).

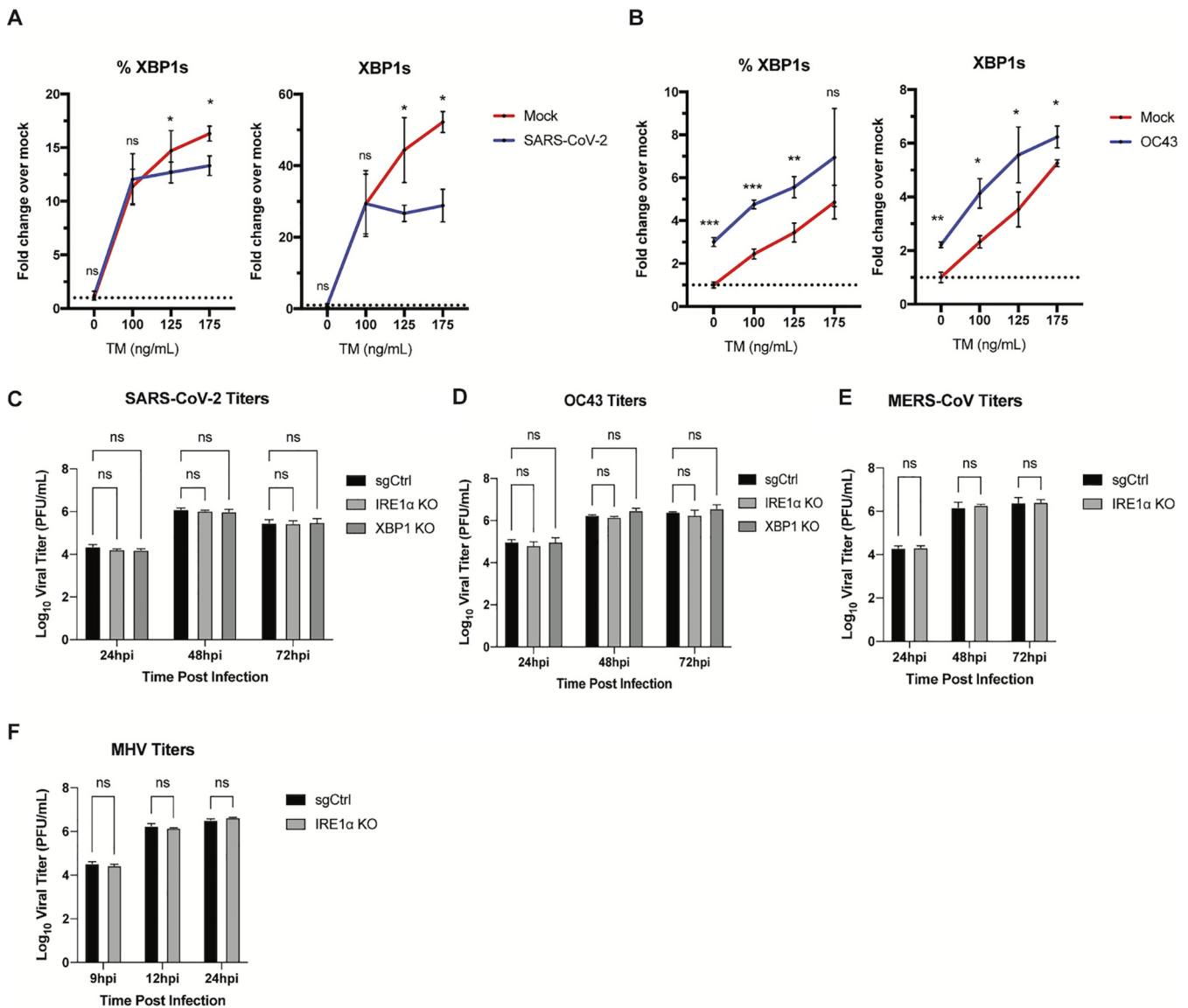


**FIG 6** SARS-CoV-2 inhibits IRE1 $\alpha$ -mediated XBP1 splicing under ER stress and does not require IRE1 $\alpha$  for replication. (A and B) A549-ACE2 cells were mock infected or infected (in triplicate) with SARS-CoV-2 (MOI, 3) (A) or OC43 (MOI, 1) (B) for 24 h prior to treatment with low doses of tunicamycin (100 to 175 ng/mL) for 6 h. Total RNA was harvested and used to quantify the relative %XBP1s and XBP1s expression by RT-qPCR.  $C_T$  values were normalized to 18S rRNA and expressed as the fold change over the mock control displayed as  $2^{-\Delta(\Delta C_T)}$ . Technical replicates were averaged, and the means for each replicate are displayed as  $\pm$ SD (error bars). Statistical significance (infected compared to mock) was determined by one-tailed, paired *t* tests (\*,  $P < 0.05$ ; \*\*,  $P < 0.01$ ; \*\*\*,  $P < 0.001$ ; ns, not significant). (C to F) Infection of CRISPR/Cas9-edited IRE1 $\alpha$  KO A549 cells with different coronaviruses. Experiments were performed using sgControl or IRE1 $\alpha$  KO or XBP1 KO (where indicated) A549 cells stably expressing viral receptors: A549-ACE2 (OC43 or SARS-CoV-2), A549-DDP4 (MERS-CoV), and A549-MHVR (MHV). Cells were infected (in triplicate) with SARS-CoV-2, MERS-CoV, OC43, or MHV at an MOI of 1. At the indicated times, supernatants were collected, and infectious virus was quantified by plaque assay. Values are means  $\pm$  SD (error bars). Statistical significance was determined by two-way ANOVA (\*,  $P < 0.05$ ; \*\*,  $P < 0.01$ ; ns, not significant). Data shown are from one representative of at least two independent experiments.

into the role of IRE1 $\alpha$  in regulating betacoronaviruses, we conducted RNA-seq analysis of sg control or IRE1 $\alpha$  knockout A549-ACE2 cells infected with either SARS-CoV-2 or OC43 compared to mock-infected cells. Infections of A549-ACE2 cells were carried out at 33°C to enable direct comparison of the two viruses (OC43 replication is significantly more robust at 33°C compared to 37°C [41], while SARS-CoV-2 replicates to a similar extent at both temperatures [Fig. S4A]). Principal-component analysis (PCA) showed a modest change in cellular gene expression upon OC43 infection of wild-type cells relative to SARS-CoV-2, which showed a robust alteration in gene expression (Fig. 7A). In contrast to uninfected or OC43-infected cells, loss of IRE1 $\alpha$  significantly impacted host gene expression in SARS-CoV-2-infected A549 cells (Fig. 7A and B). Clustering analysis

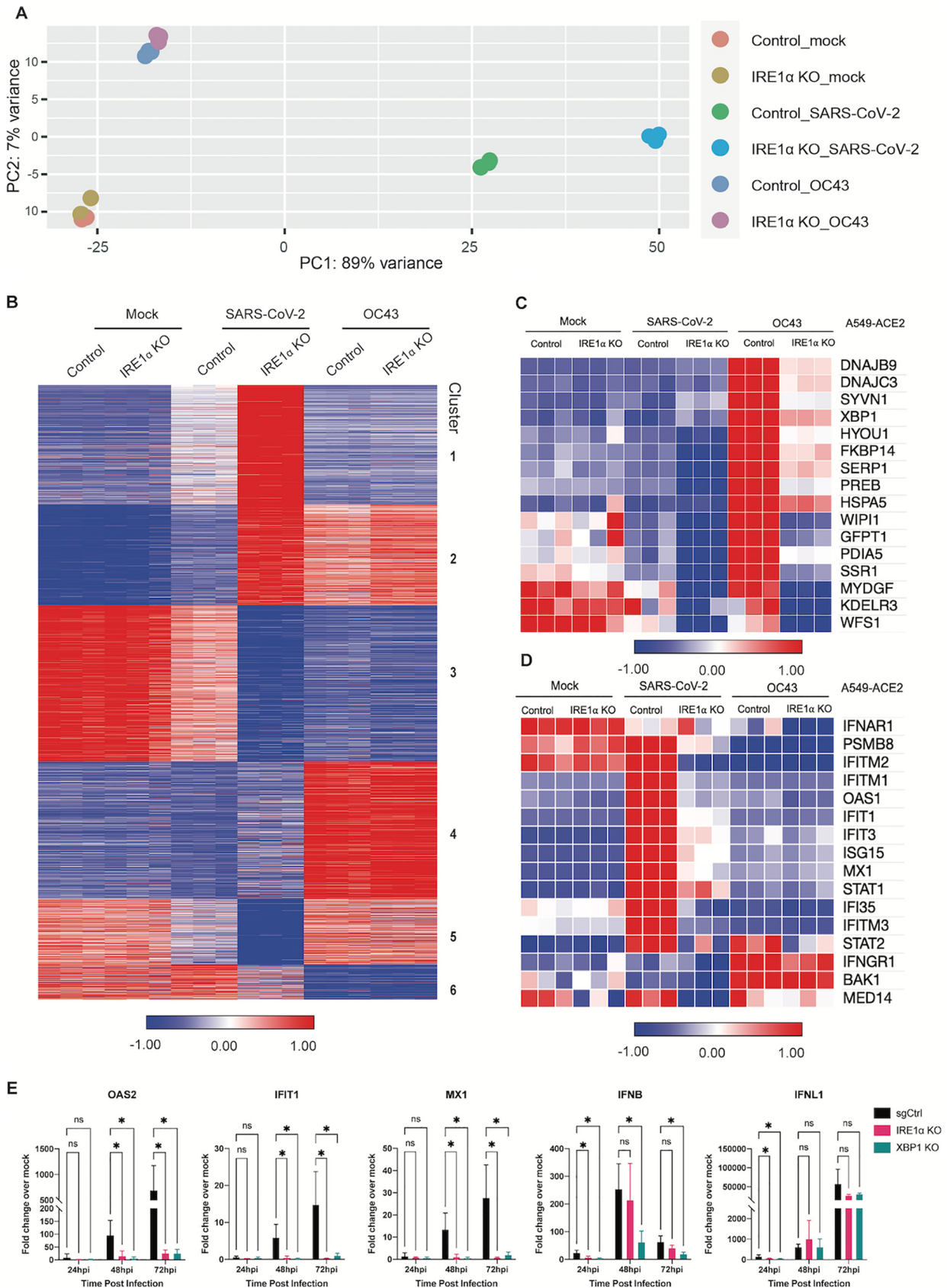


**FIG 7** IRE1α promotes the induction of interferon stimulated genes upon SARS-CoV-2 infection. (A to E) A549-ACE2 CRISPR/Cas9-edited IRE1α KO or control cells were mock infected or infected (in triplicate) with SARS-CoV-2 or OC43 (MOI 1) for 48 h. All infections were performed (Continued on next page)

of RNA-seq data revealed 6 distinct clusters altered upon loss of IRE1 $\alpha$  related to key cellular functions, including chromatin organization (cluster 1), mRNA metabolism and processing (cluster 2), and protein translation (cluster 3) (Fig. 7B and Fig. S5A). Detailed analysis of the IRE1 $\alpha$ -mediated UPR pathway confirms activation by OC43 infection that is inhibited upon loss of IRE1 $\alpha$  (Fig. 7C and Fig. S4B to E). In contrast, minimal change in this pathway was observed in SARS-CoV-2-infected cells, consistent with our previous results in this study. Loss of IRE1 $\alpha$  also appears to alter other elements of the UPR in SARS-CoV-2-infected cells, including some genes in the PERK and ATF6 pathways (Fig. S6), which may reflect compensatory effects on the UPR in an attempt to control proteostasis in the absence of IRE $\alpha$  (42–44). Strikingly, we observed significantly lower induction of some IFN-stimulated genes (ISGs) during SARS-CoV-2 infection of IRE1 $\alpha$  KO cells (Fig. 7D and Fig. S4F and S5B). We have previously reported that SARS-CoV-2 induces type I and type III IFN signaling and ISGs in multiple cell types (3). Interestingly, OC43 infection did not induce notable IFN or ISG responses with or without IRE1 $\alpha$  expression, so we were unable to make the same observations with this virus (Fig. 7D). To confirm these results, we performed RT-qPCR on representative IFN genes and ISGs genes that we have previously reported to be upregulated during SARS-CoV-2 infection (3). Consistent with our RNA-seq data, we observed significantly lower induction of ISGs such as OAS2, MX1, and IFIT1 during SARS-CoV-2 infection of cells lacking IRE1 $\alpha$  expression at both 37°C (Fig. 7E) and 33°C (Fig. S4F). These data suggest that IRE1 $\alpha$  may play a role in augmenting IFN signaling, while not being necessary for ISG induction, in SARS-CoV-2-infected cells. Our data taken together lead us to propose the model shown in Fig. 8.

## DISCUSSION

Human respiratory betacoronaviruses initiate infection in the upper respiratory tract and have the potential to cause life-threatening pneumonia as a result of infection and inflammation of the lower respiratory tract. The host response to severe infection with coronaviruses is associated with marked dysfunction in the distal lung (alveolar) epithelium, which includes disruption of barrier function, dysregulated immune responses, transcriptomic reprogramming to a transitional cell state, and senescence (45, 46).

To better understand the host epithelial response to coronavirus infection, we systematically compared the activation of the IRE1 $\alpha$ /XBP1 pathway of the UPR during infection with betacoronaviruses in lung-derived A549 and Calu-3 cells lines and iPSC-derived AT2 cells. We employed three human viruses, each from a different betacoronavirus subgenus, OC43 (embeco), SARS-CoV-2 (sarbeco) and MERS-CoV (merbeco), and included the murine coronavirus MHV, a model embecovirus. We found a striking difference between the host response to SARS-CoV-2 and the other three viruses. OC43, MHV, and MERS-CoV all activated the canonical IRE1 $\alpha$ /XBP1 pathway in both A549 and Calu-3 cell lines as evidenced by phosphorylation of IRE1 $\alpha$  (Fig. 2), XBP1 mRNA splicing (Fig. 3 and 4) and induction of DNAJB9 (Fig. 3), a transcriptional target of XBP1s. Additionally, MERS-CoV was observed to induce IRE1 $\alpha$ /XBP1 activation in iAT2 cells (Fig. 5). In contrast, while SARS-CoV-2 also promoted autophosphorylation of IRE1 $\alpha$ , there was no evidence of XBP1s, indicating that the pathway was only partially activated and suggesting that the IRE1 $\alpha$  kinase was active while the XBP1 splicing RNase activity was not. The differential splicing of XBP1 mRNA during SARS-CoV-2 and

### FIG 7 Legend (Continued)

under the same culture conditions at 33°C. Total RNA was harvested, and RNA sequencing was performed as described in Materials and Methods. (A) Principal-component analysis (PCA) of RNA-seq data from samples in triplicate. The first and second principal components (PC1 and PC2) of each sample are plotted. (B) Heatmap of normalized expression levels of the 5,000 most variable genes across all samples were plotted, and K-means clustering was used to divide genes into six clusters based on expression patterns among different treatment conditions. (C and D) Heatmap of normalized expression levels from RNA-seq of ER stress IRE1 $\alpha$ -mediated genes (C) or interferon-stimulated genes (D) for all treatment conditions. (E) Total RNA was used to quantify and validate expression of ISGs by RT-qPCR.  $C_T$  values were normalized to 18S rRNA and expressed as the fold change over the mock control displayed as  $2^{-\Delta(\Delta C_T)}$ . Technical replicates were averaged, and the means for each replicate are displayed as  $\pm$  SD (error bars). Statistical significance (infected compared to mock) was determined by ordinary one-way ANOVA (\*,  $P < 0.05$ ; \*\*,  $P < 0.01$ ; \*\*\*,  $P < 0.001$ ; \*\*\*\*,  $P < 0.0001$ ; ns, not significant).

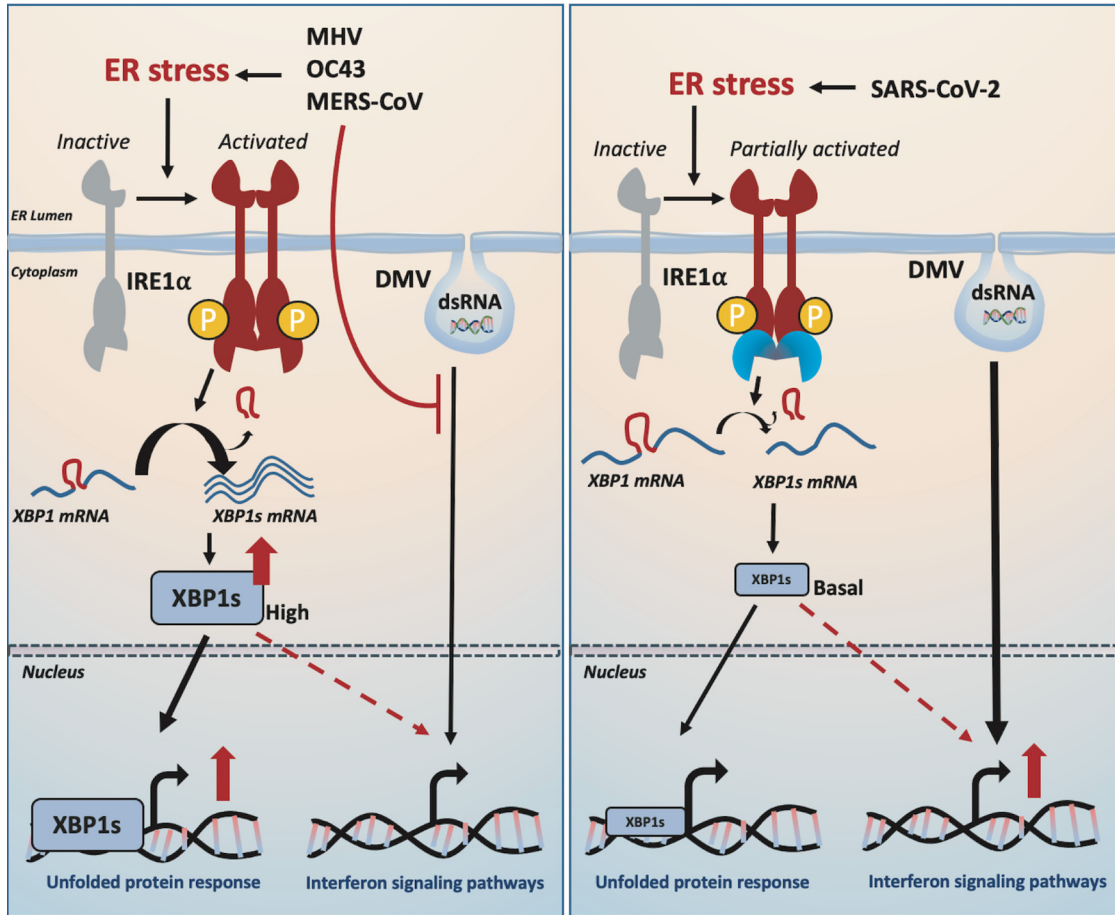


**FIG 8** Model of betacoronavirus activation of the IRE1 $\alpha$ /XBP1 pathway and downstream effects on interferon signaling. MHV, OC43, and MERS-CoV infection induces ER stress that leads to IRE1 $\alpha$  autophosphorylation and downstream IRE1 $\alpha$  RNase-mediated XBP1 splicing producing XBP1s. In contrast, SARS-CoV-2 infection only partially activates IRE1 $\alpha$  through autophosphorylation but prevents the activation of the RNase activity. XBP1s maintains a low basal level upon SARS-CoV-2 infection. MERS-CoV, OC43, and MHV efficiently antagonize dsRNA induction of IFN signaling. In contrast, SARS-CoV-2 allows dsRNA induction of some IFN signaling, and basal XBP1s potentiates the induction of IFN signaling upon SARS-CoV-2 infection.

MERS-CoV infection was also observed in iPSC-derived AT2 cells, confirming the results in a more physiologically relevant system (Fig. 5). The difference among these viruses is surprising, as all of them encode highly conserved replicase and structural proteins that promote ER membrane rearrangements and challenge the ER folding capacity, respectively (32). We had originally hypothesized that these conserved genes would induce similar stress on the ER and lead to UPR activation. Instead, our data suggest that that SARS-CoV-2 actively prevents XBP1 splicing (Fig. 6A and B). Consistent with this idea, a recombinant SARS-CoV lacking the E protein (rSARS-CoV- $\Delta$ E) was reported to induce more XBP1 splicing as well as induction of UPR genes compared to parental wild-type virus (47).

To investigate the importance of IRE1 $\alpha$  for coronavirus replication, we evaluated replication of each of the betacoronaviruses in IRE1 $\alpha$  KO A549 cells compared to parental wild-type cells. In contrast to influenza (48), all of the betacoronaviruses examined were able to replicate efficiently in the absence of IRE1 $\alpha$  signaling, consistent with a previous report of the gammacoronavirus IBV (31). While we did observe a decrease in OC43 and SARS-CoV-2 nucleocapsid expression following KIRA8 treatment (Fig. 2A and F), the similar levels of replication of all the viruses in IRE1 $\alpha$  KO cells and parental cells (Fig. 6C to F) suggest that this is due to off-target effects of KIRA8 rather than IRE1 $\alpha$  inhibition limiting virus replication. This raises interesting possibilities for the role of IRE1 $\alpha$  during coronavirus infection. As previously stated, IRE1 $\alpha$  can produce

both cytoprotective (through XBP1s) and destructive responses (via RIDD and JNK/p38 signaling) depending on the extent of the encountered stress. It seems likely that coronavirus infection would induce extensive and prolonged ER stress, which may push IRE1 $\alpha$  beyond the initial pro-recovery responses and toward a pro-apoptotic response. Indeed, our data reveal that, at least with MERS-CoV and SARS-CoV-2 infection, IRE1 $\alpha$  phosphorylation is readily detectable by 24 hpi and remains steady throughout the course of infection (Fig. S1A and B). Additionally, unlike what has been observed with chemically induced ER stress (36, 49), IRE1 $\alpha$  phosphorylation does not appear to attenuate at any point during coronavirus infection, again suggesting a hyperactive and destructive outcome. As stated above, destruction of cells, in particular, AT2 cells in the lung, may contribute to pathogenesis during coronavirus infection. However, SARS-CoV-2 appears to limit the downstream consequences of IRE1 $\alpha$  activation, most notably, XBP1 splicing via its RNase activity, and thus may be protected from this destructive phenotype. MERS-CoV may induce apoptosis redundantly in the UPR, as it has been reported that MERS-CoV induces and benefits from apoptosis mediated by the PERK arm of the UPR (27, 50).

To further probe the impact of IRE1 $\alpha$  signaling on host gene expression following coronavirus infection, we performed RNA-seq analysis of sg control or IRE1 $\alpha$  knockout A549-ACE2 cells infected with either SARS-CoV-2 or OC43. IRE1 $\alpha$  deletion significantly reduced the expression of genes downstream of XBP1s during OC43 infection, as expected, with otherwise only modest changes in overall gene expression. In contrast, genetic ablation of IRE1 $\alpha$  significantly impacted host gene expression in SARS-CoV-2-infected A549 cells. The two most dramatic effects that appear to be specific to SARS-CoV-2 relate to chromatin organization and protein folding and transport. Effects on mRNA metabolism and processing are also observed for SARS-CoV-2 and, more modestly, for OC43. Finally, protein translation is downregulated in both OC43 and SARS-CoV-2-infected cells but, in the latter case, occurs primarily upon loss of IRE1 $\alpha$ . Taken together, these results suggest that IRE1 $\alpha$  plays a key role in mediating changes in host cell gene transcription and protein production caused by SARS-CoV-2.

We found here that deletion of IRE1 $\alpha$  blunted the induction of some but not all ISGs by SARS-CoV-2 infection. In contrast, OC43 was not observed to induce significant levels of IFN or ISG mRNAs in either WT or IRE1 $\alpha$  KO cells. The mechanism by which loss of IRE1 $\alpha$  activity during SARS-CoV-2 infection dampens the induction of interferon signaling remains to be determined. It has been reported that the UPR can precede and prime innate immune signaling in flavivirus-infected cells (51). XBP1s has been found upstream of IFN $\alpha$  and IFN $\beta$  transcription and may work through binding upstream *cis*-acting enhancer elements (52, 53). Moreover, XBP1s can directly bind and transcriptionally activate interleukin-6 (IL-6), tumor necrosis factor  $\alpha$  (TNF- $\alpha$ ), and other inflammatory cytokines (54). It is possible that a low level of background XBP1 splicing may occur during SARS-CoV-2 infection, which could contribute to these responses. Independent of its RNase activity, the autophosphorylated cytoplasmic domain of IRE1 $\alpha$  can oligomerize and serve as a scaffold that recruits TRAF2, JNK, ASK, Nck, and other molecules that can lead to varied signaling outputs (55, 56). Therefore, the ability of SARS-CoV-2 to prevent full IRE1 $\alpha$  activation might dampen inflammatory signaling and prevent detection and elimination by the immune system in an intact organism. However, it is important to note that the diminution of ISG expression in the absence of IRE1 $\alpha$  is variable among ISGs, and SARS-CoV-2 still induces IFN and IFN signaling to a greater extent than OC43 in IRE1 $\alpha$  KO cells. We speculate that SARS-CoV-2 has adapted to tolerate a low level of IFN signaling as well as protein kinase R (PKR) and oligoadenylate RNase L (OAS/RNase L) activation, and the reduced ISG expression in the absence of IRE1 $\alpha$  does not have enough of an effect to promote increased replication. This is consistent with our finding that knockout of mitochondrial antiviral signaling protein (MAVS) from A549 cells, resulting in minimal IFN expression and ISG signaling, does not promote increased SARS-CoV-2 replication (3). Thus, the significance of IRE1 $\alpha$ -dependent IFN signaling is not clear and will be a subject of future investigation.

Overall, despite the lack of apparent virus replication defects with IRE1 $\alpha$  deficiency, further characterization of the repertoire of betacoronavirus-induced IRE1 $\alpha$  signaling is warranted, including contributions to cytokine production, apoptosis, and proinflammatory responses. While we initially investigated this pathway from the perspective of the impact on virus replication, future studies should examine effects of IRE1 $\alpha$  activation on the host, including inflammation and cell death through the JNK and p38 mitogen-activated protein kinase (MAPK) signaling scaffolded by IRE1 $\alpha$  (22) and/or RIDD, as a consequence of prolonged IRE1 $\alpha$  activation (17, 57). These responses could be particularly important in AT2 cells, which must rely on the UPR to maintain proteostasis in the face of the challenge from the biosynthesis and secretion of surfactant proteins (58). Dysregulation of these responses by coronavirus infection could promote AT2 cell reprogramming, epithelial apoptosis, alteration of surfactant components in alveoli, and the rampant inflammation associated with severe coronavirus infection (59–61). Finally, the UPR response is complex and made up of the PERK and ATF6 pathways in addition to IRE1 $\alpha$ , and signals from all three of these pathways almost certainly integrate into the final outcome of an infected cell. Indeed, changes in the PERK and ATF6 pathways may compensate for the IRE1 $\alpha$  deficiency in the KO cells and explain the absence of an effect on replication of any of the betacoronaviruses under study.

We recently reported that SARS-CoV-2 and MERS-CoV also diverge in their activation and antagonism of the dsRNA-induced host cell innate immune responses, another early innate response to viruses (3). While MERS-CoV actively antagonizes type I and type III interferon production and signaling, the oligoadenylate RNase L (OAS/RNase L) system and the PKR pathway, SARS-CoV-2 activates OAS/RNase L and PKR and induces a low level of IFN and ISG expression (3, 4) in A549 and Calu-3 respiratory tract-derived cells. Here, we observed that OC43 infection did not lead to the induction of IFN or ISGs (Fig. 7D), and we have shown previously that OC43-encoded accessory protein NS2 antagonizes activation of the OAS/RNase L pathway (62). Activation of these pathways during MERS-CoV mutant infection significantly reduces virus replication (63), while SARS-CoV-2 can tolerate the innate responses activated during infection (3).

Considering the differences we have observed between betacoronaviruses with innate immune responses and now IRE1 $\alpha$  activation and signaling, it is striking that MERS-CoV and SARS-CoV-2 are reciprocal in what they activate and antagonize. To optimize replication, coronaviruses must likely strike a balance in the cellular responses they antagonize, tolerate, or benefit from. Supporting this, our data suggest that IRE1 $\alpha$  influences ISG induction during infection. It is intriguing to consider if MERS-CoV tolerates this by antagonizing IFN and ISG induction, while SARS-CoV-2 instead limits IRE1 $\alpha$  activity. Future studies should examine the synergy between innate immune responses and the UPR during coronavirus infection and how perturbations on one side may change viral replicative capacity, tropism, and spread. Understanding how signals from each one of these pathways are integrated into viral replication and cell fate decisions during coronavirus infection may illuminate new therapeutic strategies for combating emerging betacoronaviruses.

## MATERIALS AND METHODS

**Cell lines.** Human A549 cells (ATCC CCL-185) and its derivatives were cultured in RPMI 1640 (Gibco catalog no. 11875) supplemented with 10% fetal bovine serum (FBS), 100 U/mL penicillin, and 100  $\mu$ g/mL streptomycin (Gibco catalog no. 15140). African green monkey kidney Vero cells (E6) (ATCC CRL-1586) and VeroCCL81 cells (ATCC CCL-81) were cultured in Dulbecco's modified Eagle's medium (DMEM; Gibco catalog no. 11965) supplemented with 10% FBS, 100 U/mL of penicillin, 100  $\mu$ g/mL streptomycin, 50  $\mu$ g/mL gentamicin (Gibco catalog no. 15750), 1 mM sodium pyruvate (Gibco catalog no. 11360), and 10 mM HEPES (Gibco catalog no. 15630). Human HEK 293T cells (ATCC CRL-3216) were cultured in DMEM supplemented with 10% FBS. Human Calu-3 cells (ATCC HTB-55) were cultured in DMEM supplemented with 20% FBS without antibiotics. Mouse L2 cells (64) were grown in DMEM supplemented with 10% FBS, 100 U/mL penicillin, 100  $\mu$ g/mL streptomycin, 10 nM HEPES, 2 mM L-glutamine (Gibco catalog no. 25030081), and 2.5  $\mu$ g/mL amphotericin B (Gibco catalog no. 15290).

A549-DPP4 (4), A549-ACE2 (3), and A549-MHVR (4) cells were generated as described previously. A549-ACE2 cells, used in Fig. 3I and J, Fig. 4, Fig. 6, and Fig. S3 were a kind gift of Benjamin TenOever, Mt. Sinai Icahn School of Medicine. CRISPR-Cas9 knockout cell lines were generated using lentiviruses.

**TABLE 1** Antibodies

| Primary antibody      | Antibody species | Blocking buffer <sup>a</sup> | Dilution | Catalog no.                       |
|-----------------------|------------------|------------------------------|----------|-----------------------------------|
| Phospho-IRE1 $\alpha$ | Rabbit           | 5% BSA/TBST                  | 1:1,000  | Abcam EPR5253 Invitrogen PA585738 |
| IRE1 $\alpha$ (14C10) | Rabbit           | 5% Milk/TBST                 | 1:1,000  | Cell Signaling Technology 32945   |
| XBP1s                 | Mouse            | 5% Milk/TBST                 | 1:1,000  | BioLegend 9D11A43                 |
| GAPDH (14C10)         | Rabbit           | 5% Milk/TBST                 | 1:2,000  | Cell Signaling Technology 2118S   |
| SARS-CoV-2 N          | Rabbit           | 5% Milk/TBST                 | 1:2,000  | Gentex GTX135357                  |
| MERS-CoV N            | Mouse            | 5% Milk/TBST                 | 1:2,000  | Sino Biological40068-MM10         |
| OC43 N                | Rabbit           | 5% Milk/TBST                 | 1:2,000  | Sino Biological 40643-T62         |

<sup>a</sup>TBST, Tris-buffered saline with Tween 20.

Lentivirus stocks were generated by using lentiCRISPR v2 (Addgene) with single guide RNA (sgRNA) targeting IRE1 $\alpha$  sequences (version 1 [V1]: CGGTCACTACCCCGAGGCC, V2: TTCAGGAAGCGTCACTGTGC, V3: CGGTCACTACCCCGAGGCC) or XBP1 sequence (TCGAGCCTTCTTCGATCTC). The infected A549-ACE2 cells were polyclonally selected and maintained by culture in medium supplemented with 4  $\mu$ g/mL puromycin for 1 week.

iPSC (SPC2 iPSC line, clone SPC2-ST-B2, Boston University)-derived alveolar epithelial type 2 cells (iAT2) were grown and infected as previously described (3). In brief, cells were differentiated and maintained as alveolospheres embedded in 3D Matrigel in CK+DCI medium, as previously described (65). For generation of 2D alveolar cells for viral infection, alveolospheres were dispersed into single cells and then plated on precoated 1/30 Matrigel plates at a cell density of 125,000 cells/cm<sup>2</sup> using CK+DCI medium with ROCK inhibitor for the first 48 h, and then the medium was changed to CK+DCI medium at day 3 and either mock infected or infected with MERS-CoV or SARS-CoV-2 at an MOI of 5.

**Viruses.** SARS-CoV-2 (USA-WA1/2020) was obtained from BEI Resources, NIAID, NIH or provided by Natalia Thornburg, World Reference Center for Emerging Viruses and Arboviruses (Galveston, Texas) and propagated in VeroE6-TMPRSS2 cells. The genomic RNA was sequenced and found to be identical to that of GenBank version no. [MN985325.1](#). Recombinant MERS-CoV was described previously (1) and propagated in VeroCCL81 cells. SARS-CoV-2 and MERS-CoV infections were performed at the University of Pennsylvania or at the Howard Taylor Ricketts Laboratory (HTRL) at Argonne National Laboratory (Lemont, IL) in biosafety level 3 (BSL-3) laboratories under BSL-3 conditions, using appropriate and approved personal protective equipment and protocols. OC43 was obtained from ATCC (VR-1558) and grown and titrated on VeroE6 cells at 33°C or on A549-mRuby cells as previously described (66). MHV-A59 (5, 67) was propagated on A549-MHVR cells or on murine 17CL-1 cells.

**Viral growth kinetics and titration.** SARS-CoV-2 and MERS-CoV infections and plaque assays were performed as previously described (1, 5). In brief, A549 cells were seeded at  $3 \times 10^5$  cells per well in a 12-well plate for infections. Calu-3 cells were seeded similarly onto rat tail collagen type I-coated plates (Corning no. 356500). Cells were washed once with phosphate-buffered saline (PBS) before being infected with virus diluted in serum-free medium—RPMI for A549 cells or DMEM for Calu-3 cells. Virus was absorbed for 1 h (A549 cells) or 2 h (Calu-3 cells) at 37°C before the cells were washed 3 times with PBS and the medium was replaced with 2% FBS RPMI (A549 cells) or 4% FBS DMEM (Calu-3 cells). At the indicated time points, 200  $\mu$ L of medium was collected to quantify released virus by plaque assay and stored at  $-80^\circ\text{C}$ . Infections for MHV growth curves were performed similarly under BSL-2 conditions. For OC43 infections, similar infection conditions and media were used; however, virus was absorbed, and the infections were incubated at 33°C rather than 37°C.

Plaque assays were performed using VeroE6 cells for SARS-CoV-2 and OC43, VeroCCL81 cells for MERS-CoV, and L2 cells for MHV. SARS-CoV-2 and MERS-CoV plaque assays were performed in 12-well plates at 37°C. OC43 and MHV plaque assays were performed in 6-well plates at 33°C and 37°C, respectively. In all cases, virus was absorbed onto cells for 1 h at the indicated temperatures before overlay was added. For SARS-CoV-2, MERS-CoV, and OC43 plaque assays, a liquid overlay was used (DMEM with 2% FBS, 1 $\times$  sodium pyruvate, and 0.1% agarose). A solid overlay was used for MHV plaque assays (DMEM plus 2% FBS, 1 $\times$  HEPES, 1 $\times$  glutamine, 1 $\times$  Fungizone, and 0.7% agarose). Cell monolayers were fixed with 4% paraformaldehyde and stained with 1% crystal violet after the following incubation times: SARS-CoV-2 and MERS-CoV, 3 days; OC43, 5 days; MHV, 2 days. All plaque assays were performed in biological triplicate and technical duplicate.

**Pharmacologic agents.** KIRA8 was purchased at >98% purity from Chemveda Life Sciences India Pvt. Ltd. For use in tissue culture, KIRA8 stock solution was prepared by dissolving in dimethyl sulfoxide (DMSO). Tunicamycin (catalog no. T7765) and Tg (catalog no. T9033) were purchased at >98% purity from Sigma. For use in tissue culture, tunicamycin and TG stock solutions were prepared by dissolving in DMSO.

**Immunoblotting.** Cells were washed once with ice-cold PBS, and lysates were harvested at the indicated times post infection with lysis buffer (1% NP-40, 2 mM EDTA, 10% glycerol, 150 mM NaCl, 50 mM Tris HCl, pH 8.0) supplemented with protease inhibitors (Roche complete mini-EDTA-free protease inhibitor) and phosphatase inhibitors (Roche PhosStop easy pack). After 5 min, lysates were incubated on ice for 20 min and centrifuged for 20 min at 4°C, and supernatants were mixed 3:1 with 4 $\times$  Laemmli sample buffer (Bio-Rad 1610747). Samples were heated at 95°C for 5 min and then separated on SDS-PAGE and transferred to polyvinylidene difluoride (PVDF) membranes. Blots were blocked with 5% nonfat milk or



5% bovine serum albumin (BSA) and probed with antibodies (Table 1) diluted in the same blocking buffer. Primary antibodies were incubated overnight at 4°C or for 1 h at room temperature. All secondary antibody incubation steps were done for 1 h at room temperature. Blots were visualized using Thermo Scientific SuperSignal chemiluminescent substrates (catalog no. 34095 or 34080). The antibodies are listed in Table 1.

**RNA sequencing.** A549 cells expressing the MERS-CoV receptor DPP4 (4) were cultured in 10% FBS RPMI medium. At 70% cell confluence, cells were washed once with PBS before being mock infected or infected with MERS-CoV (EMC/2012) at an MOI of 1. Virus was absorbed for 1 h at 37°C in serum-free RPMI medium. After 1 h, virus was removed, cells were washed three times with PBS, and 2% FBS RPMI was added. The cells were incubated for another 24 h or 36 h and then washed once with PBS and lysed using RLT Plus lysis buffer before genomic DNA removal and total RNA extraction using the Qiagen RNeasy Plus minikit (Qiagen 74134). Three independent biological replicates were performed per experimental condition. RNA sample quality check, library construction, and sequencing were performed with GeneWiz following standard protocols. All samples were sequenced using an Illumina HiSeq sequencer to generate paired-end 150-bp reads. Read quality was assessed using FastQC v0.11.2 as described in reference 68. Raw sequencing reads from each sample were quality and adapter trimmed using BBDuk 38.73 as described in reference 69. The reads were mapped to the human genome (hg38 with Ensembl v98 annotation) using RNA STAR v2.7.1a (70). The resulting BAM files were counted with featureCounts v1.6.4 to count the number of reads for each gene (71). Differential expression between mock, 24 hpi, and 36 hpi experimental conditions were analyzed using the raw gene counts files by DESeq2 v1.22.1 (72). A PCA plot of RNA-seq samples and a normalized gene expression matrix were also generated with DESeq2.

For SARS-CoV-2 and OC43 infections, ACE2-A549 sg control or IRE1 KO cells were cultured in 10% FBS RPMI to 70% confluence. Cells were washed once with PBS before being mock infected or infected with each virus at an MOI of 1 for 1 h in serum-free RPMI at 33°C. Cells were then washed three times with PBS before 2% FBS RPMI was added. At 48 hpi, cells were lysed with RLT Plus lysis buffer before genomic DNA removal and total RNA extraction using the Qiagen RNeasy Plus minikit (Qiagen 74134). Three independent biological replicates were performed per experimental condition. RNA sample quality check, library construction, and sequencing were performed by the University of Chicago Genomics Facility following standard protocols. All samples were sequenced in two runs using a NovaSeq 6000 sequencer to generate paired-end 100-bp reads. For each sample, the reads from two flow cells were combined before downstream processing. Quality and adapter trimming were performed on the raw sequencing reads using TrimGalore v0.6.3 (<https://github.com/FelixKrueger/TrimGalore>). The reads were mapped to the human genome (UCSC hg19 with GENCODE annotation), and the downstream analyses were performed using the same methods as described above.

**Host pathway activity analysis of viruses.** RNA-seq data from Gene Expression Omnibus (GEO) no. GSE147507 (37), GSE168797 (38), and GSE144882 (35) and the data presented herein were used to compare the effects of different viruses on host ER stress response. Specifically, Ingenuity Pathway Analysis (IPA) (<https://digitalinsights.qiagen.com/products-overview/discovery-insights-portfolio/analysis-and-visualization/qiagen-ipa/>) was used to predict activities of related canonical pathways based on host gene expression changes following viral infection. Activation Z-scores for every virus and canonical pathway combination were plotted as a heatmap using Morpheus (<https://software.broadinstitute.org/morpheus>). IPA used the following *q* value cutoffs for each data set to perform the canonical pathway cross-comparison: Calu-3 SARS-CoV-2 MOI 2 24 h *q* < 0.05, NHBE SARS-CoV-2 MOI 2 24 h *q* < 0.1, A549-ACE2 SARS-CoV-2 MOI 0.2 24 h *q* < 0.1, A549-ACE2 SARS-CoV-2 MOI 2 24 h *q* < 0.05, A549-ACE2 SARS-CoV-2 MOI 3 24 h *q* < 0.01, A549-ACE2 SARS-CoV-2 MOI 1 48 h 33°C *q* < 0.05, A549-ACE2 OC43 MOI 1 48 h 33°C *q* < 0.001, A549-DPP4 MERS-CoV MOI 1 24 h *q* < 0.1, A549-DPP4 MERS-CoV MOI 1 36 h *q* < 0.01, BMDM MHV-A59 MOI 1 12 h *q* < 0.1 and over 1-fold up- or downregulated. These cutoffs were implemented due to the limitations set by the IPA software. IPA was also used to overlay gene expression data (log<sub>2</sub> fold change) onto the interferon signaling pathway map (Fig. S5B).

**Gene expression heatmaps.** Expression levels for genes involved in various pathways from RNA-seq data were drawn using Morpheus. For each gene, the normalized expression values of all samples were transformed by subtracting the mean and dividing by the standard deviation. The transformed gene expression values were used to generate the heatmap. For the clustering analysis of RNA-seq experiments for OC43- and SARS-CoV-2-infected A549-ACE2 cells with or without IRE1 $\alpha$ , the top 5,000 most variable genes were selected. The normalized gene expression data were analyzed using Morpheus. K-means clustering with 6 clusters was applied to the gene expression data.

**Gene set enrichment analyses.** To identify themes across the 6 clusters, functional gene set enrichment analyses for the genes in each cluster were performed using Metascape (73). The following categories were selected for the enrichment analyses: GO molecular functions, GO biological processes, and KEGG pathway. Metascape analysis was performed with a minimum *P* value significance threshold of 0.05, a minimum overlap of 10 genes, and a minimum enrichment score of 5. Notable pathways enriched by Metascape from each cluster were summarized in a heatmap using Morpheus. GSEA v4.1.0 (74) was used to perform specific gene set enrichment analyses on Gene Ontology terms: IRE1-mediated unfolded protein response (75, 76), response to type I interferon (77), and response to interferon alpha (78) using the normalized expression data from the RNA-seq experiment for OC43- and SARS-CoV-2-infected A549-ACE2 cells with or without IRE1 $\alpha$ .

**Statistical analysis.** All statistical analyses and plotting of data were performed using GraphPad Prism software. RT-qPCR data were analyzed by Student's *t* test. Plaque assay data were analyzed by

**TABLE 2** Primer sequences

| Target sequence                   | Forward primer (5' to 3') | Reverse primer (5' to 3') |
|-----------------------------------|---------------------------|---------------------------|
| XBP1s                             | GCTGAGTCCGCAGCAGGT        | CTGGGTCCAAGTTGCCAGAAT     |
| XBP1 total                        | TGAAAACAGAGTAGCAGCTCAGA   | CCCAAGCGCTGTCTTAACTC      |
| RPL13A                            | CTCAAGGTGTTTGACGGCATCC    | TACTTCCAGCCAACCTCGTGAG    |
| 18S rRNA                          | TTCGATGGTAGTCGCTGTGC      | CTGCTGCCTTCCTTGAATGTGGTA  |
| SARS-CoV-2 genome<br>(nsp12/RdRp) | GGTAACTGGTATGATTTTCG      | CTGGTCAAGGTTAATATAGG      |
| MERS-CoV genome (nsp7)            | GCACATCTGTGGTTCTCCTCTCT   | AAGCCCCAGGCCCTACTATTAGC   |
| DNAJB9                            | AGTCGGAGGGTGCAGGATATT     | TTGATTTGGCGCTCTGATGC      |

two-way analysis of variance (ANOVA) with multiple-comparison correction. Displayed significance is determined by the *P* value; \*, *P* < 0.05; \*\*, *P* < 0.01; \*\*\*, *P* < 0.001; \*\*\*\*, *P* < 0.0001; ns, not significant.

**Quantification of XBP1 alternative splicing using RNA-seq data.** BAM files produced using RNA STAR were analyzed in Integrative Genomics Viewer v2.9.4 to count the number of XBP1 reads containing the alternative splicing (79). The total number of XBP1 reads was counted with featureCounts. The percentage of XBP1 alternative splicing for each sample was determined by dividing the number of alternatively spliced reads by the number of total XBP1 reads (spliced plus unspliced).

**Quantitative PCR (RT-qPCR).** Cells were lysed with RLT Plus buffer, and total RNA was extracted using the RNeasy Plus minikit (Qiagen). RNA was reverse transcribed into cDNA with a high-capacity cDNA reverse transcriptase kit (Applied Biosystems 4387406). cDNA samples were diluted in molecular biology-grade water and amplified using specific RT-qPCR primers (see Table 2). RT-qPCR experiments were performed on a Roche LightCycler 96 instrument. SYBR green supermix was from Bio-Rad. Host gene expression displayed as the fold change over mock-infected samples was generated by first normalizing cycle threshold ( $C_T$ ) values to 18S rRNA to generate  $\Delta C_T$  values ( $\Delta C_T = C_T$  gene of interest  $- C_T$  18S rRNA). Next,  $\Delta$  ( $\Delta C_T$ ) values were determined by subtracting the mock-infected  $\Delta C_T$  values from the virus-infected samples. Technical triplicates were averaged and means displayed using the equation  $2^{-\Delta(\Delta C_T)}$ . Primer sequences are listed in Table 2.

**XBP1 splicing assay by RT-qPCR.** RT-qPCR was used to quantify the relative expression of the spliced version of XBP1 (XBP1s) by using specific pairs of primers for human alternatively spliced XBP1 and total XBP1 (primer sequences are described above) as previously described (80). The relative percentage of alternative splicing of XBP1 (%XBP1s) was indicated by calculating the ratio of signals between XBP1s and total XBP1.

**Data availability.** Raw and processed RNA-seq data for MERS-CoV, OC43, and SARS-CoV-2 were deposited in the Gene Expression Omnibus database ([GSE193169](https://www.ncbi.nlm.nih.gov/geo/query/acc.cgi?acc=GSE193169)).

## SUPPLEMENTAL MATERIAL

Supplemental material is available online only.

**FIG S1**, PDF file, 0.3 MB.

**FIG S2**, PDF file, 0.05 MB.

**FIG S3**, PDF file, 0.6 MB.

**FIG S4**, PDF file, 1.2 MB.

**FIG S5**, PDF file, 1.3 MB.

**FIG S6**, PDF file, 0.2 MB.

## ACKNOWLEDGMENTS

We thank Alejandra Fausto for help with OC43 propagation and titration and Darrell Kotton (Boston University) and Rachel Truitt and the Penn iPSC Core for preparation of the iAT2 cells. We thank the members of SARS-CoV-2 host response team in Chicago for stimulating discussions and support, particularly Julian Solway, Rick Morimoto, Nissim Hay, Raymond Roos, and Dominique Missiakas. We thank the University of Chicago Genomics Facility (RRID:SCR\_019196), especially Pieter Faber, for their assistance with RNA-seq.

This work was supported by National Institutes of Health grant R01-AI140442 and supplement for SARS-CoV-2 (S.R.W.), R01CA219815 (S.A.O.), R01EY027810 (S.A.O.), U01DK127786 (S.A.O.), R01 GM121735 (M.R.R.); Department of Veterans Affairs Merit Review 2I01BX005411 (M.F.B. and S.R.W.); Penn Center for Research on Coronaviruses and Other Emerging Pathogens (S.R.W.); BIG Vision grant from the University of Chicago (M.R.R.); and NIH P30 CA014599 (University of Chicago Comprehensive Cancer Center Support grant). D.M.R. was supported in part by National Institutes of Health T32AI055400. D.Y. was supported in part by the Frank W. and Shirley D. Fitch Scholarship Fund.

S.R.W. is on the scientific advisory boards of Immunome, Inc., and Ocugen, Inc. S.A.O. is a cofounder and consultant at OptiKira, L.L.C. (Cleveland, OH). R.E.M. is a founder and consultant at ReAx Biotechnologies (Chicago, IL) and Anastasis Biotech (London, UK).

## REFERENCES

- Fehr AR, Perlman S. 2015. Coronaviruses: an overview of their replication and pathogenesis. *Methods Mol Biol* 1282:1–23. [https://doi.org/10.1007/978-1-4939-2438-7\\_1](https://doi.org/10.1007/978-1-4939-2438-7_1).
- Gorbalenya AE, Enjuanes L, Ziebuhr J, Snijder EJ. 2006. Nidovirales: evolving the largest RNA virus genome. *Virus Res* 117:17–37. <https://doi.org/10.1016/j.virusres.2006.01.017>.
- Li Y, Renner DM, Comar CE, Whelan JN, Reyes HM, Cardenas-Diaz FL, Truitt R, Tan LH, Dong B, Alysandratos KD, Huang J, Palmer JN, Adappa ND, Kohanski MA, Kotton DN, Silverman RH, Yang W, Morrissey EE, Cohen NA, Weiss SR. 2021. SARS-CoV-2 induces double-stranded RNA-mediated innate immune responses in respiratory epithelial-derived cells and cardiomyocytes. *Proc Natl Acad Sci U S A* 118:e2022643118. <https://doi.org/10.1073/pnas.2022643118>.
- Comar CE, Goldstein SA, Li Y, Yount B, Baric RS, Weiss SR. 2019. Antagonism of dsRNA-induced innate immune pathways by NS4a and NS4b accessory proteins during MERS coronavirus infection. *mBio* 10:e00319-19. <https://doi.org/10.1128/mBio.00319-19>.
- Zhao L, Jha BK, Wu A, Elliott R, Ziebuhr J, Gorbalenya AE, Silverman RH, Weiss SR. 2012. Antagonism of the interferon-induced OAS-RNase L pathway by murine coronavirus ns2 protein is required for virus replication and liver pathology. *Cell Host Microbe* 11:607–616. <https://doi.org/10.1016/j.chom.2012.04.011>.
- Rabouw HH, Langereis MA, Knaap RCM, Dalebout TJ, Canton J, Sola I, Enjuanes L, Bredenbeek PJ, Kikkert M, de Groot RJ, van Kuppeveld FJM. 2016. Middle East respiratory coronavirus accessory protein 4a inhibits PKR-mediated antiviral stress responses. *PLoS Pathog* 12:e1005982. <https://doi.org/10.1371/journal.ppat.1005982>.
- de Wilde AH, Wansee KF, Scholte FEM, Goeman JJ, Ten Dijke P, Snijder EJ, Kikkert M, van Hemert MJ. 2015. A kinome-wide small interfering RNA screen identifies proviral and antiviral host factors in severe acute respiratory syndrome coronavirus replication, including double-stranded RNA-activated protein kinase and early secretory pathway proteins. *J Virol* 89:8318–8333. <https://doi.org/10.1128/JVI.01029-15>.
- Kikkert M. 2020. Innate immune evasion by human respiratory RNA viruses. *J Innate Immun* 12:4–20. <https://doi.org/10.1159/000503030>.
- Cruz JLG, Becares M, Sola I, Oliveros JC, Enjuanes L, Zúñiga S. 2013. Alpha-coronavirus protein 7 modulates host innate immune response. *J Virol* 87:9754–9767. <https://doi.org/10.1128/JVI.01032-13>.
- Zhao J, Falcón A, Zhou H, Netland J, Enjuanes L, Pérez Breña P, Perlman S. 2009. Severe acute respiratory syndrome coronavirus protein 6 is required for optimal replication. *J Virol* 83:2368–2373. <https://doi.org/10.1128/JVI.02371-08>.
- Kindler E, Thiel V, Weber F. 2016. Interaction of SARS and MERS coronaviruses with the antiviral interferon response. *Adv Virus Res* 96:219–243. <https://doi.org/10.1016/bs.aivir.2016.08.006>.
- Fung TS, Huang M, Liu DX. 2014. Coronavirus-induced ER stress response and its involvement in regulation of coronavirus-host interactions. *Virus Res* 194:110–123. <https://doi.org/10.1016/j.virusres.2014.09.016>.
- Fung TS, Liu DX. 2014. Coronavirus infection, ER stress, apoptosis and innate immunity. *Front Microbiol* 5:296.
- Travers KJ, Patil CK, Wodicka L, Lockhart DJ, Weissman JS, Walter P. 2000. Functional and genomic analyses reveal an essential coordination between the unfolded protein response and ER-associated degradation. *Cell* 101:249–258. [https://doi.org/10.1016/S0092-8674\(00\)80835-1](https://doi.org/10.1016/S0092-8674(00)80835-1).
- Zhang K, Kaufman RJ. 2006. The unfolded protein response: a stress signaling pathway critical for health and disease. *Neurology* 66:S102–S109. <https://doi.org/10.1212/01.wnl.0000192306.98198.ec>.
- Harding HP, Calton M, Urano F, Novoa I, Ron D. 2002. Transcriptional and translational control in the mammalian unfolded protein response. *Annu Rev Cell Dev Biol* 18:575–599. <https://doi.org/10.1146/annurev.cellbio.18.011402.160624>.
- Han D, Lerner AG, Vande Walle L, Upton J-P, Xu W, Hagen A, Backes BJ, Oakes SA, Papa FR. 2009. IRE1 $\alpha$  kinase activation modes control alternate endoribonuclease outputs to determine divergent cell fates. *Cell* 138:562–575. <https://doi.org/10.1016/j.cell.2009.07.017>.
- Ghosh R, Wang L, Wang ES, Perera BGK, Igbaria A, Morita S, Prado K, Thamsen M, Caswell D, Macias H, Weiberth KF, Gliedt MJ, Alavi MV, Hari SB, Mitra AK, Bhatarai B, Schürer SC, Snapp EL, Gould DB, German MS, Backes BJ, Maly DJ, Oakes SA, Papa FR. 2014. Allosteric inhibition of the IRE1 $\alpha$  RNase preserves cell viability and function during endoplasmic reticulum stress. *Cell* 158:534–548. <https://doi.org/10.1016/j.cell.2014.07.002>.
- Calton M, Zeng H, Urano F, Till JH, Hubbard SR, Harding HP, Clark SG, Ron D. 2002. IRE1 couples endoplasmic reticulum load to secretory capacity by processing the XBP-1 mRNA. *Nature* 415:92–96. <https://doi.org/10.1038/415092a>.
- Yoshida H, Matsui T, Yamamoto A, Okada T, Mori K. 2001. XBP1 mRNA is induced by ATF6 and spliced by IRE1 in response to ER stress to produce a highly active transcription factor. *Cell* 107:881–891. [https://doi.org/10.1016/S0092-8674\(01\)00611-0](https://doi.org/10.1016/S0092-8674(01)00611-0).
- Lee AH, Iwakoshi NN, Glimcher LH. 2003. XBP-1 regulates a subset of endoplasmic reticulum resident chaperone genes in the unfolded protein response. *Mol Cell Biol* 23:7448–7459. <https://doi.org/10.1128/MCB.23.21.7448-7459.2003>.
- Hetz C. 2012. The unfolded protein response: controlling cell fate decisions under ER stress and beyond. *Nat Rev Mol Cell Biol* 13:89–102. <https://doi.org/10.1038/nrm3270>.
- Upton J-P, Wang L, Han D, Wang ES, Huskey NE, Lim L, Truitt M, McManus MT, Ruggero D, Goga A, Papa FR, Oakes SA. 2012. IRE1 $\alpha$  cleaves select microRNAs during ER stress to derepress translation of proapoptotic Caspase-2. *Science* 338:818–822. <https://doi.org/10.1126/science.1226191>.
- Chakrabarti A, Jha BK, Silverman RH. 2011. New insights into the role of RNase L in innate immunity. *J Interferon Cytokine Res* 31:49–57. <https://doi.org/10.1089/jir.2010.0120>.
- He B. 2006. Viruses, endoplasmic reticulum stress, and interferon responses. *Cell Death Differ* 13:393–403. <https://doi.org/10.1038/sj.cdd.4401833>.
- Bechill J, Chen Z, Brewer JW, Baker SC. 2008. Coronavirus infection modulates the unfolded protein response and mediates sustained translational repression. *J Virol* 82:4492–4501. <https://doi.org/10.1128/JVI.00017-08>.
- Sims AC, Mitchell HD, Gralinski LE, Kyle JE, Burnum-Johnson KE, Lam M, Fulcher ML, West A, Smith RD, Randell SH, Metz TO, Sheahan TP, Waters KM, Baric RS. 2021. Unfolded protein response inhibition reduces Middle East respiratory syndrome coronavirus-induced acute lung injury. *mBio* 12:e0157221. <https://doi.org/10.1128/mBio.01572-21>.
- Echavarría-Consuegra L, Cook GM, Busnadiego I, Lefèvre C, Keep S, Brown K, Doyle N, Dowgier G, Franaszek K, Moore NA, Siddell SG, Bickerton E, Hale BG, Firth AE, Brierley I, Irigoyen N. 2021. Manipulation of the unfolded protein response: a pharmacological strategy against coronavirus infection. *PLoS Pathog* 17:e1009644. <https://doi.org/10.1371/journal.ppat.1009644>.
- Prestes EB, Bruno JCP, Travassos LH, Carneiro LAM. 2021. The unfolded protein response and autophagy on the crossroads of coronavirus infections. *Front Cell Infect Microbiol* 11:668034. <https://doi.org/10.3389/fcimb.2021.668034>.
- Favreau DJ, Desforges M, St-Jean JR, Talbot PJ. 2009. A human coronavirus OC43 variant harboring persistence-associated mutations in the S glycoprotein differentially induces the unfolded protein response in human neurons as compared to wild-type virus. *Virology* 395:255–267. <https://doi.org/10.1016/j.virol.2009.09.026>.
- Fung TS, Liao Y, Liu DX. 2014. The endoplasmic reticulum stress sensor IRE1 $\alpha$  protects cells from apoptosis induced by the coronavirus infectious bronchitis virus. *J Virol* 88:12752–12764. <https://doi.org/10.1128/JVI.02138-14>.
- Wang Y, Grunewald M, Perlman S. 2020. Coronaviruses: an updated overview of their replication and pathogenesis. *Methods Mol Biol* 2203:1–29. [https://doi.org/10.1007/978-1-0716-0900-2\\_1](https://doi.org/10.1007/978-1-0716-0900-2_1).
- Chan C-P, Siu K-L, Chin K-T, Yuen K-Y, Zheng B, Jin D-Y. 2006. Modulation of the unfolded protein response by the severe acute respiratory syndrome coronavirus spike protein. *J Virol* 80:9279–9287. <https://doi.org/10.1128/JVI.00659-06>.
- Rashid F, Dzakah EE, Wang H, Tang S. 2021. The ORF8 protein of SARS-CoV-2 induced endoplasmic reticulum stress and mediated immune

- evasion by antagonizing production of interferon beta. *Virus Res* 296:198350. <https://doi.org/10.1016/j.virusres.2021.198350>.
35. Volk A, Hackbart M, Deng X, Cruz-Pulido Y, O'Brien A, Baker SC. 2020. Coronavirus endoribonuclease and deubiquitinating interferon antagonists differentially modulate the host response during replication in macrophages. *J Virol* 94:e00178-20. <https://doi.org/10.1128/JVI.00178-20>.
  36. Chang T-K, Lawrence DA, Lu M, Tan J, Harnoss JM, Marsters SA, Liu P, Sandoval W, Martin SE, Ashkenazi A. 2018. Coordination between two branches of the unfolded protein response determines apoptotic cell fate. *Mol Cell* 71:629–636.e625. <https://doi.org/10.1016/j.molcel.2018.06.038>.
  37. Blanco-Melo D, Nilsson-Payant BE, Liu W-C, Uhl S, Hoagland D, Møller R, Jordan TX, Oishi K, Panis M, Sachs D, Wang TT, Schwartz RE, Lim JK, Albrecht RA, tenOever BR. 2020. Imbalanced host response to SARS-CoV-2 drives development of COVID-19. *Cell* 181:1036–1045.e1039. <https://doi.org/10.1016/j.cell.2020.04.026>.
  38. Nguyen LC, Yang D, Nicolaescu V, Best TJ, Ohtsuki T, Chen S-N, Friesen JB, Drayman N, Mohamed A, Dann C, Silva D, Gula H, Jones KA, Millis M, Dickinson BC, Tay S, Oakes SA, Pauli GF, Meltzer DO, Randall G, Rosner MR. 2021. Cannabidiol inhibits SARS-CoV-2 replication and promotes the host innate immune response. *bioRxiv*. <https://doi.org/10.1101/2021.03.10.432967>.
  39. Arabi YM, Balkhy HH, Hayden FG, Bouchama A, Luke T, Baillie JK, Al-Omari A, Hajjeer AH, Senga M, Denison MR, Nguyen-Van-Tam JS, Shindo N, Bermingham A, Chappell JD, Van Kerkhove MD, Fowler RA. 2017. Middle East respiratory syndrome. *N Engl J Med* 376:584–594. <https://doi.org/10.1056/NEJMs1408795>.
  40. Bridges JP, Vladar EK, Huang H, Mason RJ. 2022. Respiratory epithelial cell responses to SARS-CoV-2 in COVID-19. *Thorax* 77:203–209. <https://doi.org/10.1136/thoraxjnl-2021-217561>.
  41. Bucknall RA, King LM, Kapikian AZ, Chanock RM. 1972. Studies with human coronaviruses. II. Some properties of strains 229E and OC43. *Proc Soc Exp Biol Med* 139:722–727. <https://doi.org/10.3181/00379727-139-36224>.
  42. Moore PC, Qi JY, Thamsen M, Ghosh R, Peng J, Gliedt MJ, Meza-Acevedo R, Warren RE, Hiniker A, Kim GE, Maly DJ, Backes BJ, Papa FR, Oakes SA. 2019. Parallel signaling through IRE1 $\alpha$  and PERK regulates pancreatic neuroendocrine tumor growth and survival. *Cancer Res* 79:6190–6203. <https://doi.org/10.1158/0008-5472.CAN-19-1116>.
  43. Walter F, O'Brien A, Concannon CG, Dussmann H, Prehn JHM. 2018. ER stress signaling has an activating transcription factor 6 $\alpha$  (ATF6)-dependent “off-switch. *J Biol Chem* 293:18270–18284. <https://doi.org/10.1074/jbc.RA118.002121>.
  44. Vandewynckel Y-P, Laukens D, Bogaerts E, Paridaens A, Van den Bussche A, Verhelst A, Van Steenkiste C, Descamps B, Vanhove C, Libbrecht L, De Rycke R, Lambrecht BN, Geerts A, Janssens S, Van Vlierberghe H. 2015. Modulation of the unfolded protein response impedes tumor cell adaptation to proteotoxic stress: a PERK for hepatocellular carcinoma therapy. *Hepatology* 9:93–104. <https://doi.org/10.1007/s12072-014-9582-0>.
  45. D'Agnillo F, Walters K-A, Xiao Y, Sheng Z-M, Scherler K, Park J, Gygli S, Rosas LA, Sadtler K, Kalish H, Blattl CA, Zhu R, Gatzke L, Bushell C, Memoli MJ, O'Day SJ, Fischer TD, Hammond TC, Lee RC, Cash JC, Powers ME, O'Keefe GE, Butnor KJ, Rapkiewicz AV, Travis WD, Layne SP, Kash JC, Taubenberger JK. 2021. Lung epithelial and endothelial damage, loss of tissue repair, inhibition of fibrinolysis, and cellular senescence in fatal COVID-19. *Sci Transl Med* 13:eabj7790. <https://doi.org/10.1126/scitranslmed.abj7790>.
  46. Melms JC, Biermann J, Huang H, Wang Y, Nair A, Tagore S, Katsyv I, Rendeiro AF, Amin AD, Schapiro D, Frangieh CJ, Luoma AM, Filliol A, Fang Y, Ravichandran H, Clausi MG, Alba GA, Rogava M, Chen SW, Ho P, Montoro DT, Kornberg AE, Han AS, Bakhroum MF, Anandasabapathy N, Suárez-Fariñas M, Bakhroum SF, Bram Y, Borczuk A, Guo XV, Lefkowitz JH, Marboe C, Lagana SM, Del Portillo A, Tsai EJ, Zorn E, Markowitz GS, Schwabe RF, Schwartz RE, Elemento O, Saqi A, Hibshoosh H, Que J, Izar B. 2021. A molecular single-cell lung atlas of lethal COVID-19. *Nature* 595:114–119. <https://doi.org/10.1038/s41586-021-03569-1>.
  47. DeDiego ML, Nieto-Torres JL, Jiménez-Guardaño JM, Regla-Nava JA, Alvarez E, Oliveros JC, Zhao J, Fett C, Perlman S, Enjuanes L. 2011. Severe acute respiratory syndrome coronavirus envelope protein regulates cell stress response and apoptosis. *PLoS Pathog* 7:e1002315. <https://doi.org/10.1371/journal.ppat.1002315>.
  48. Hassan IH, Zhang MS, Powers LS, Shao JQ, Baltrusaitis J, Rutkowski DT, Legge K, Monick MM. 2012. Influenza A viral replication is blocked by inhibition of the inositol-requiring enzyme 1 (IRE1) stress pathway. *J Biol Chem* 287:4679–4689. <https://doi.org/10.1074/jbc.M111.284695>.
  49. Li H, Korenykh AV, Behrman SL, Walter P. 2010. Mammalian endoplasmic reticulum stress sensor IRE1 signals by dynamic clustering. *Proc Natl Acad Sci U S A* 107:16113–16118. <https://doi.org/10.1073/pnas.1010580107>.
  50. Chu H, Shuai H, Hou Y, Zhang X, Wen L, Huang X, Hu B, Yang D, Wang Y, Yoon C, Wong VH-Y, Li C, Zhao X, Poon VK-M, Cai J-P, Wong KK-Y, Yeung M-L, Zhou J, Au-Yeung RK-H, Yuan S, Jin D-Y, Kok K-H, Perlman S, Chan JF-W, Yuen K-Y. 2021. Targeting highly pathogenic coronavirus-induced apoptosis reduces viral pathogenesis and disease severity. *Sci Adv* 7:eabf8577. <https://doi.org/10.1126/sciadv.abf8577>.
  51. Carletti T, Zakaria MK, Faoro V, Reale L, Kazungu Y, Licastro D, Marcello A. 2019. Viral priming of cell intrinsic innate antiviral signaling by the unfolded protein response. *Nat Commun* 10:3889. <https://doi.org/10.1038/s41467-019-11663-2>.
  52. Beisel C, Ziegler S, Martrus Zapater G, Chapel A, Griesbeck M, Hildebrandt H, Lohse AW, Altfeld M. 2017. TLR7-mediated activation of XBP1 correlates with the IFN $\alpha$  production in humans. *Cytokine* 94:55–58. <https://doi.org/10.1016/j.cyto.2017.04.006>.
  53. Zeng L, Liu Y-P, Sha H, Chen H, Qi L, Smith JA. 2010. XBP-1 couples endoplasmic reticulum stress to augmented IFN- $\beta$  induction via a cis-acting enhancer in macrophages. *J Immunol* 185:2324–2330. <https://doi.org/10.4049/jimmunol.0903052>.
  54. Smith JA. 2018. Regulation of cytokine production by the unfolded protein response; implications for infection and autoimmunity. *Front Immunol* 9:422. <https://doi.org/10.3389/fimmu.2018.00422>.
  55. Adams CJ, Kopp MC, Larburu N, Nowak PR, Ali MMU. 2019. Structure and molecular mechanism of ER stress signaling by the unfolded protein response signal activator IRE1. *Front Mol Biosci* 6:11. <https://doi.org/10.3389/fmolb.2019.00011>.
  56. Urano F, Wang X, Bertolotti A, Zhang Y, Chung P, Harding HP, Ron D. 2000. Coupling of stress in the ER to activation of JNK protein kinases by transmembrane protein kinase IRE1. *Science* 287:664–666. <https://doi.org/10.1126/science.287.5453.664>.
  57. Hollien J, Weissman JS. 2006. Decay of endoplasmic reticulum-localized mRNAs during the unfolded protein response. *Science* 313:104–107. <https://doi.org/10.1126/science.1129631>.
  58. Katzen J, Beers MF. 2020. Contributions of alveolar epithelial cell quality control to pulmonary fibrosis. *J Clin Invest* 130:5088–5099. <https://doi.org/10.1172/JCI139519>.
  59. Yamamoto Y, Ohtori A. 1990. In vitro study of aldose reductase inhibitor concentrations in the lens and inhibitory effect on sugar alcohol accumulation. *Curr Eye Res* 9:421–428. <https://doi.org/10.3109/02713689008999607>.
  60. Maguire JA, Mulugeta S, Beers MF. 2012. Multiple ways to die: delineation of the unfolded protein response and apoptosis induced by surfactant protein C BRICHOS mutants. *Int J Biochem Cell Biol* 44:101–112. <https://doi.org/10.1016/j.biocel.2011.10.003>.
  61. Katzen J, Wagner BD, Venosa A, Kopp M, Tomer Y, Russo SJ, Headen AC, Basil MC, Stark JM, Mulugeta S, Detering RR, Beers MF. 2019. An SFTPC BRICHOS mutant links epithelial ER stress and spontaneous lung fibrosis. *JCI Insight* 4:e126125. <https://doi.org/10.1172/jci.insight.126125>.
  62. Goldstein SA, Thornbrough JM, Zhang R, Jha BK, Li Y, Elliott R, Quiroz-Figueroa K, Chen AI, Silverman RH, Weiss SR. 2017. Lineage A betacoronavirus NS2 proteins and the homologous Torovirus Berne pp1a carboxy-terminal domain are phosphodiesterases that antagonize activation of RNase L. *J Virol* 91:e02201-16. <https://doi.org/10.1128/JVI.02201-16>.
  63. Comar CE, Otter CJ, Pfannenstiel J, Doerger E, Renner DM, Tan LH, Perlman S, Cohen NA, Fehr AR, Weiss SR. 2022. MERS-CoV endoribonuclease and accessory proteins jointly evade host innate immunity during infection of lung and nasal epithelial cells. *Proc Natl Acad Sci U S A* 119:e2123208119. <https://doi.org/10.1073/pnas.2123208119>.
  64. Gombold JL, Hingley ST, Weiss SR. 1993. Fusion-defective mutants of mouse hepatitis virus A59 contain a mutation in the spike protein cleavage signal. *J Virol* 67:4504–4512. <https://doi.org/10.1128/JVI.67.8.4504-4512.1993>.
  65. Jacob A, Vedaie M, Roberts DA, Thomas DC, Villacorta-Martin C, Alysandratos K-D, Hawkins F, Kotton DN. 2019. Derivation of self-renewing lung alveolar epithelial type II cells from human pluripotent stem cells. *Nat Protoc* 14:3303–3332. <https://doi.org/10.1038/s41596-019-0220-0>.
  66. Drayman N, DeMarco JK, Jones KA, Azizi S-A, Froggatt HM, Tan K, Maltseva NI, Chen S, Nicolaescu V, Dvorkin S, Furlong K, Kathayat RS, Firpo MR, Mastrodomenico V, Bruce EA, Schmidt MM, Jedrzejczak R, Muñoz-Alía MÁ, Schuster B, Nair V, Han K-Y, O'Brien A, Tomatsidou A, Meyer B, Vignuzzi M, Missiakas D, Botten JW, Brooke CB, Lee H, Baker SC, Mounce BC, Heaton NS, Severson WE, Palmer KE, Dickinson BC, Joachimiak A, Randall G, Tay S. 2021. Masitinib is a broad coronavirus 3CL

- inhibitor that blocks replication of SARS-CoV-2. *Science* 373:931–936. <https://doi.org/10.1126/science.abg5827>.
67. Shulla A, Gallagher T. 2009. Role of spike protein endodomains in regulating coronavirus entry. *J Biol Chem* 284:32725–32734. <https://doi.org/10.1074/jbc.M109.043547>.
  68. Andrews, S. 2010. FastQC: a quality control tool for high throughput sequence data. <http://www.bioinformatics.babraham.ac.uk/projects/fastqc/>.
  69. Bushnell B. 2014. BBTools software package. <http://sourceforge.net/projects/bbmap>.
  70. Dobin A, Davis CA, Schlesinger F, Drenkow J, Zaleski C, Jha S, Batut P, Chaisson M, Gingeras TR. 2013. STAR: ultrafast universal RNA-seq aligner. *Bioinformatics* 29:15–21. <https://doi.org/10.1093/bioinformatics/bts635>.
  71. Liao Y, Smyth GK, Shi W. 2014. featureCounts: an efficient general purpose program for assigning sequence reads to genomic features. *Bioinformatics* 30:923–930. <https://doi.org/10.1093/bioinformatics/btt656>.
  72. Love MI, Huber W, Anders S. 2014. Moderated estimation of fold change and dispersion for RNA-seq data with DESeq2. *Genome Biol* 15:550. <https://doi.org/10.1186/s13059-014-0550-8>.
  73. Zhou Y, Zhou B, Pache L, Chang M, Khodabakhshi AH, Tanaseichuk O, Benner C, Chanda SK. 2019. Metascape provides a biologist-oriented resource for the analysis of systems-level datasets. *Nat Commun* 10:1523. <https://doi.org/10.1038/s41467-019-09234-6>.
  74. Subramanian A, Tamayo P, Mootha VK, Mukherjee S, Ebert BL, Gillette MA, Paulovich A, Pomeroy SL, Golub TR, Lander ES, Mesirov JP. 2005. Gene set enrichment analysis: a knowledge-based approach for interpreting genome-wide expression profiles. *Proc Natl Acad Sci U S A* 102:15545–15550. <https://doi.org/10.1073/pnas.0506580102>.
  75. Hetz C, Martinon F, Rodriguez D, Glimcher LH. 2011. The unfolded protein response: integrating stress signals through the stress sensor IRE1 $\alpha$ . *Physiol Rev* 91:1219–1243. <https://doi.org/10.1152/physrev.00001.2011>.
  76. Takaoka A, Yanai H. 2006. Interferon signalling network in innate defence. *Cell Microbiol* 8:907–922. <https://doi.org/10.1111/j.1462-5822.2006.00716.x>.
  77. Pestka S, Krause CD, Walter MR. 2004. Interferons, interferon-like cytokines, and their receptors. *Immunol Rev* 202:8–32. <https://doi.org/10.1111/j.0105-2896.2004.00204.x>.
  78. Li Q, Zhang M, Kumar S, Zhu LJ, Chen D, Bagchi MK, Bagchi IC. 2001. Identification and implantation stage-specific expression of an interferon-alpha-regulated gene in human and rat endometrium. *Endocrinology* 142:2390–2400. <https://doi.org/10.1210/endo.142.6.8101>.
  79. Robinson JT, Thorvaldsdóttir H, Winckler W, Guttman M, Lander ES, Getz G, Mesirov JP. 2011. Integrative genomics viewer. *Nat Biotechnol* 29:24–26. <https://doi.org/10.1038/nbt.1754>.
  80. Yoon S-B, Park Y-H, Choi S-A, Yang H-J, Jeong P-S, Cha J-J, Lee S, Lee SH, Lee J-H, Sim B-W, Koo B-S, Park S-J, Lee Y, Kim Y-H, Hong JJ, Kim J-S, Jin YB, Huh J-W, Lee S-R, Song B-S, Kim S-U. 2019. Real-time PCR quantification of spliced X-box binding protein 1 (XBP1) using a universal primer method. *PLoS One* 14:e0219978. <https://doi.org/10.1371/journal.pone.0219978>.